Molecular Neurobiology
https://doi.org/10.1007/s12035-024-04267-5

RESEARCH

Gastrodin Ameliorates Post-Stroke Depressive-Like Behaviors Through Cannabinoid-1 Receptor-Dependent PKA/RhoA Signaling Pathway

Shiquan Wang[1,2] · Liang Yu[3] · Haiyun Guo[2] · Wenqiang Zuo[2] · Yaru Guo[2] · Huiqing Liu[2] · Jiajia Wang[2] · Jin Wang[2] · Xia Li[4] · Wugang Hou[2] · Minghui Wang[2]

Received: 25 November 2023 / Accepted: 26 May 2024

Abstract

Post-stroke depression (PSD) is a significant complication in stroke patients, increases long-term mortality, and exaggerates ischemia-induced brain injury. However, the underlying molecular mechanisms and effective therapeutic targets related to PSD have remained elusive. Here, we employed an animal behavioral model of PSD by combining the use of middle cerebral artery occlusion (MCAO) followed by spatial restraint stress to study the molecular underpinnings and potential therapies of PSD. Interestingly, we found that sub-chronic application of gastrodin (Gas), a traditional Chinese medicinal herb *Gastrodia elata* extraction, relieved depression-related behavioral deficits, increased the impaired expression of synaptic transmission-associated proteins, and restored the altered spine density in hippocampal CA1 of PSD animals. Furthermore, our results indicated that the anti-PSD effect of Gas was dependent on membrane cannabinoid-1 receptor (CB1R) expression. The contents of phosphorated protein kinase A (p-PKA) and phosphorated Ras homolog gene family member A (p(ser188)-RhoA) were decreased in the hippocampus of PSD-mice, which was reversed by Gas treatment, and CB1R depletion caused a diminished efficacy of Gas on p-PKA and p-RhoA expression. In addition, the anti-PSD effect of Gas was partially blocked by PKA inhibition or RhoA activation, indicating that the anti-PSD effect of Gas is associated with the CB1R-mediated PKA/RhoA signaling pathway. Together, our findings revealed that Gas treatment possesses protective effects against the post-stroke depressive-like state; the CB1R-involved PKA/RhoA signaling pathway is critical in mediating Gas's anti-PSD potency, suggesting that Gas application may be beneficial in the prevention and adjunctive treatment of PSD.

Keywords Post-stroke Depression · Gastrodin · Cannabinoid-1 Receptor · PKA · RhoA · Hippocampus

Introduction

Post-stroke depression (PSD) is a common and frequent sequela of ischemic stroke. It is positively associated with slow functional rehabilitation, impaired cognitive function, poor life quality, and high mortality after stroke. Despite epidemiological investigations showing that the incidence rate of PSD was as high as 41% within two years following ischemic stroke [1], the underlying etiological mechanisms, as well as effective therapeutic targets related to PSD, largely remain elusive. This is mainly attributed to the poor understanding of the possible mechanistic insights into ischemic injuries [2, 3]. Elucidation of the molecular underpinnings and exploration of novel rational treatments for PSD are urgently needed [4, 5].

Gastrodin (Gas, $C_{13}H_{18}O_7$, has a molecular weight of 286.28. The chemical structure is shown in Fig. S1A.)is the active ingredient extracted from the dried rhizome of

Shiquan Wang, Liang Yu and Haiyun Guo contributed equally to this work.

✉ Xia Li
lixia_fmmu@163.com

✉ Wugang Hou
gangwuhou@163.com

✉ Minghui Wang
wangmh222@outlook.com

[1] College of Life Sciences, Northwest University, Xi'an 710127, Shaanxi, China

[2] Department of Anesthesiology and Perioperative Medicine, Xijing Hospital, Fourth Military Medical University, Xi'an 710032, Shaanxi, China

[3] Department of Information, Xijing Hospital, Fourth Military Medical University, Xi'an 710032, Shaanxi, China

[4] Department of Neurosurgery, Xijing Hospital, Fourth Military Medical University, Xi'an 710032, Shaanxi, China

Published online: 10 June 2024

Gastrodia elata Blume [6]. Previous studies have shown that Gas possesses numerous pharmacological activities, including analgesic, hypnotic, memory-improving, and antidepressant [7–15]. Over the past few years, both preclinical and clinical studies have provided evidence supporting the potential of Gas in treating PSD. Li et al. examined the effects of Gas on 5-HT levels and neurotrophic factors in blood. Their results indicated Gas as an effective treatment for PSD with minimal side effects [16. On the other hand, Zhao et al. explored a novel strategy to measure multiple neurotransmitters in PSD rodents, revealing Gas's analogous regulatory effect on brain neurotransmitters compared to fluoxetine in treating PSD [17]. While both studies demonstrated Gas's effectiveness in alleviating PSD-related symptoms, they primarily investigated endogenous neurotransmission-related factors and blood pharmacokinetics of Gas. These studies suggest that targeting the Gas-related signaling pathway could be a viable therapeutic strategy for PSD, However, despite the accumulating evidence, the underlying molecular and neurobiological mechanisms responsible for the anti-PSD effect of Gas need further elucidation, thereby promoting its application in clinical practice.

Substantial evidence supports the multifactorial nature of PSD, with neurobiological elements emerging as primary contributors, encompassing both genetic and environmental factors [2, 18, 19]. Studies highlight the involvement of specific candidate genes associated with depression in the development of PSD [1]. Notably, the cannabinoid-1 receptor (CB1R), widely distributed in neuroanatomical structures linked to depression, plays a pivotal role, with disrupted expression robustly implicated in depression pathogenesis [20–24]. Recent research underscores CB1R deficiency as an essential substrate for depression [25]. Furthermore, studies indicate that CB1R modulates depressive-like behaviors and support the CB1R agonists to have antidepressant effects [26, 27]. Intriguingly, Gas exhibits sedative and hypnotic effects akin to endogenous cannabinoids [12–14], making it conceivable that Gas could act on CB1R, thereby exerting an anti-PSD effect.

Recent preclinical studies have found a regulatory relationship between CB1R and the RhoA (ras homolog gene family, member A) signaling pathway. RhoA is a small G-protein that modulates various biological processes, including axonal development, dendritic branching, and synaptogenesis [28–30]. Several studies have confirmed that RhoA plays a vital role in PSD [31, 32]. Previous reports revealed that CB1R acts as axon guidance cues and regulates synaptogenesis by activating the RhoA-related pathway [33], indicating the involvement of RhoA in CB1R-induced neurodevelopment. In addition, PKA (protein kinase A), an essential regulatory molecule of RhoA, regulates the expression level of RhoA and the activity of RhoA through phosphorylation [34, 35]. Recent studies confirmed that Gas could activate PKA [36], and activation of PKA has an antidepressant effect [37, 38]. Therefore, we hypothesized that Gas ameliorates post-stroke depressive-like behaviors by restoring the spine morphogenesis disruption and stabilizing the expression pattern of synaptic proteins in the hippocampus; the CB1R/PKA/RhoA pathway is involved in this process.

While the mouse MCAO model has been extensively employed to investigate brain ischemia, it is noted that mice in this model typically do not manifest spontaneous depressive-like symptoms post-stroke. However, when combined with a sub-threshold spatial restraint stress-typically insufficient to induce depressive-like behaviors in mice-the MCAO mice consistently develop behavioral deficits that replicate core features of real-world stroke-induced hemiplegia-related depressive symptoms, including despair and anhedonia [39]. This model offers an ideal avenue for investigating the mechanisms underlying behavioral changes in stressed MCAO mice, providing vital insights into understanding human PSD. In this study, we investigated the spatial restraint stress-induced depressive-like behavioral changes following ischemic stroke. Our investigation delved into the functional relevance of spine morphogenesis and the expression patterns of CB1R, PKA, and RhoA proteins in the context of post-stroke depressive-like behaviors. Additionally, we explored the therapeutic potential of Gas in mitigating the generation and progression of depressive-like behaviors in stressed MCAO mice. Our findings shed light on the molecular mechanisms underpinning PSD pathogenesis and underscore the beneficial therapeutic effects of Gas in alleviating post-stroke depression.

Materials and Methods

Experimental Design

First, to validate the effect of Gas on behavioral changes in stressed MCAO mice, animals were randomly assigned to seven groups: Sham, Sham + SRS, Saline, Gas-50, Gas-100, Gas-200, and Fluoxetine groups. In the Sham group, animals received no treatment. In the sham + SRS group, spatial restraint stress was imposed for 21 days and no other operations were performed. In the saline group, spatial restraint stress was initiated 7 days after MCAO, followed by intravenous injection of saline (5 ml/kg) starting from 28 days after cerebral ischemia, once daily for 7 consecutive days. In the Gas-50, Gas-100, and Gas-200 groups, spatial restraint stress was performed 7 days after MCAO. Gas (purity 99.7%, synthesized and analyzed for purity by Kunming Pharmaceutical Group, China. This drug was commercially obtained in the form of a gastrodin injection, with a registered approval number for

drugs: Sinopharm H20013046, supplied in aliquots of 0.2 g × 2 ml 0.9% saline per vial) was intravenously administrated at dosages of 50 mg/kg, 100 mg/kg, and 200 mg/kg, respectively, starting 28 days after MCAO, once daily for one week. In the Fluoxetine group, fluoxetine (Solarbio Life Sciences, SF8500) was intraperitoneally administrated at a dosage of 20 mg/kg once daily for one week. Depressive-like behavioral performance, dendritic spine density, and dendrite complexity were analyzed. Synaptic plasticity-related proteins and the level of CB1R in the hippocampus were detected in the fifth week after the stroke.

Next, to elucidate the role of CB1R in Gas-mediated anti-PSD effect, we employed mice with locally knocked-out CB1R in the hippocampus. Animals were randomly assigned to three groups: Gas, Gas + mCherry, and Gas + Cre. The Gas group received 100 mg/kg Gas administration. In the Gas + mCherry group, MCAO was performed on CB1R-flox$^{+/+}$ mice, spatial restraint stress was executed 7 days after MCAO, and 100 mg/kg Gas was intravenously administrated starting from 28 days after cerebral ischemia, once daily for 7 consecutive days. In the Gas + Cre group, MCAO was performed on mice with locally knocked-out CB1R, spatial restraint stress was performed 7 days after MCAO, and 100 mg/kg Gas was intravenously administrated starting from 28 days after cerebral ischemia, once daily for 7 consecutive days. Depressive-like behavioral performance, dendritic spine density, and dendrite complexity were analyzed. Synaptic plasticity-related proteins were detected in the fifth week after the stroke in the hippocampus.

In the third part, to assess the impact of the Gas application on the PKA/RhoA signaling pathway, animals were randomly assigned to five groups: Sham, Saline, Gas only, Gas + mCherry, and Gas + Cre. The treatment of the Sham and Saline groups was the same as in part one, while the treatment of Gas, Gas + mCherry and Gas + Cre groups was the same as in part two. Western blotting was used to detect p-PKA, PKA, p-RhoA, and RhoA expression patterns. Additionally, we verified the anti-PSD effect of Gas under conditions regulating PKA/RhoA activity. Animals were randomly allocated to four groups: Gas + saline, Gas + H89, Gas + DMSO, and Gas + U46619. Depressive-like behavioral performance, synaptic plasticity-related proteins, dendritic spine density, and dendrite complexity were analyzed in the fifth week after the stroke in the hippocampus.

Animals

Male C57BL/6 mice (8–10 weeks old, 20–22 g) were housed with an environmental temperature of 22 ± 2ºC and humidity of 50 ± 1% with ad libitum access to food and water. Animals were purchased from the Experimental Animal Center of Air Force Military University (former The Fourth Military Medical University). All experimental protocols were approved and conducted in strict adherence to the regulations and guidelines of Air Force Military University Institutional Animal Care, following the AAALAC, and in accordance with the Institutional Animal Care and Use Committee guidelines, the ethical approval number is IACUC-20220350 and the approval date is March 10, 2022.

Transient Cerebral Ischemia and Reperfusion

As previously described [40], transient focal cerebral ischemia was induced using an intraluminal monofilament occlusion of the middle cerebral artery (MCAO). Briefly, mice were anesthetized with isoflurane (1.5%, 20,181,501, RWD Life Science), and rectal temperature was monitored using a probe, maintaining it at 37 ± 0.5ºC. The blood flow to the right MCA was abruptly interrupted using a specialized MCAO suture (RWD Life Science), and blood flow blockage was sustained for one hour. Subsequently, the suture was carefully withdrawn to restore blood flow. A laser Doppler sensor (Periflux System 5010, PERIMED) was positioned on the skull surface (2 mm caudal, 4 mm lateral right to bregma) to monitor the regional cerebral blood flow rate. Animals exhibiting an 80% decrease and 70% recovery within this range of blood flow were selected as ischemic stroke mice and subjected to subsequent experiments. Successful stroke modeling was confirmed by detecting cerebral blood flow at different stages during MCAO operation using a laser speckle imaging system (RFLSI III+, RWD Apparatus), 2,3,5-triphenyl tetrazolium chloride (TTC) staining was conducted on randomly selected mice 7 days following the middle cerebral artery occlusion (MCAO) procedure to corroborate the cerebral blood flow changes identified through laser speckle imaging. Images obtained from Sham mice that did not undergo the MCAO procedure were considered as the control condition (Fig. S1B, C). The MCAO mice, together with Sham mice, were then randomly assigned to different experimental groups for subsequent procedures.

Spatial Restraint Stress

Spatial restraint stress was performed based on a previous report [39]. Briefly, 7 days after MCAO surgery, mice were individually placed into custom-made ventilated tubes for 3 h daily (from 2:30 pm to 5:30 pm) without being able to turn the body around for 21 consecutive days.

Open Field Test

A cohort of 8 mice was subjected to an open field test 28 days after MCAO to assess the impact of MCAO on animals' motor activity. Mice were individually placed in the center of a non-transparency plexiglass-constructed open field box

(40 cm × 40 cm × 30 cm) and allowed to move freely for a 5-minute video-tracked period. Movement traces were stored in a Windows 10 operating system PC and analyzed using ANY-maze software (Stoelting).

Sucrose Preference Test

Mice were allowed to consume two bottles of solutions in individual cages for 24 h, one with 1% sucrose (w/v) (Sigma, S9378) and the other with drinking water. The positions of the two bottles were exchanged at 12 h intervals to avoid the development of position preference. Before testing started, all mice were subjected to water deprivation for 24 h and then were allowed to consume 100 ml bottled water and 100 ml 1% bottled sucrose for 24 h. The sucrose preference index was defined as (volume of consumed sucrose) / (volume of consumed sucrose + volume of consumed water) ×100%.

Forced Swim Test

The forced swim test (FST) was conducted as previously described [41]. Experimental mice were individually handled and placed into a plastic cylinder (30 cm high with a 20 cm diameter) containing 15 cm water depth for 15 min as a pretest assessment. 24 h later, the behavioral performance of each mouse in FST was video monitored for 6 min. The immobility time for the last 4 min was calculated when mice stopped struggling or made a minimum movement to keep floating in the water.

Tail Suspension Test

As previously narrated, mice were individually suspended within a rectangular compartment (45 cm high with a 15 cm depth) [42]. Behavioral performance was video monitored for 6 min. An experimenter analyzed the duration of immobility blindly according to the defined criteria.

Molecular Docking

Molecular docking was performed using Autodock 5 software, and Discovery Studio 2019 was utilized for diagram visualization. The molecular dock predicts binding modes by profiling the property characteristics of CB1R and Gas and speculating their binding activity.

Immunofluorescence Staining

Mice were perfused transcardially with 20 ml of PBS, then fixation with 4% ice-cold paraformaldehyde. Brains were dissected and post-fixed at 4 ℃ for 6 ~ 8 h and dehydrated in 30% sucrose, frozen brain tissues were cut into 15-μm-thick coronal cerebral sections with a Leica cryostat (Leica CM1950, Leica Biosystems). Sections were processed in PBS for 10 min, treated with 10% normal donkey serum in PBST (PBS + 0.3% Triton X-100) for 30 min, and then incubated with the following primary antibodies at 4℃ overnight: Goat anti-CB1R (1:100, ab108319, Abcam), guinea pig anti-NeuN (1:300, 266,004, Synaptic Systems). Next, the sections were incubated with secondary antibodies (1:500) for 2 h and washed three times with PBS. Finally, the sections were washed and mounted. Alexa 594-conjugated goat anti-guinea pig (A11076, Thermo-Fisher) and Alexa 488-conjugated donkey anti-rabbit (ab150064, Abcam) were used. Sections were imaged using a confocal microscope (Fluoview FV1200, Olympus) with identical parameters.

Plasma Membrane Protein Extraction

Membrane protein was extracted by Minute ™ membrane protein extraction kit (Invent Biotechnologies, INC). In brief, ipsilateral hippocampus tissue on day 35 after MCAO was dissected on ice after overdose euthanasia with isoflurane. The tissue samples were homogenized in 2–3 volumes of buffer A until completely lysed (30–50 min). Then transfer the supernatant to a new vial and centrifuge at 10,000 g for 30 min at 4℃. Collect the pellet and discard the supernatant, resuspend the pellet in 50–200 μl buffer B for 30 min at 4℃, and centrifuge at 10,000 g for 30 min at 4℃. Last, collect the supernatant and store it at -80℃ for later uses (this concludes membrane-bound protein).

Western Blotting

After excessive euthanasia with isoflurane, ipsilateral hippocampus tissue was dissected on ice 35 days after MCAO. The samples were then lysed with RIPA buffer (Beyotime) containing a proteinase inhibitor cocktail. A BCA protein assay kit (Beyotime) validated the protein concentration. The protein samples were run on 10% SDS-PAGE gels and then transferred to polyvinylidene difluoride membranes (Millipore). Membranes were blocked with 5% bovine serum albumin for 1 h, the membranes were then cut horizontally based on the molecular weight of the corresponding protein. Primary antibodies were used at the following dilutions: rabbit anti-PKA (1:1000, 4782 S, Cell Signaling Technology), rabbit anti-p-PKA (1:500, 9621 S, Cell Signaling Technology), anti-RhoA (1:1000, 2117, Cell Signaling Technology), anti-p(S188)RhoA (1:500, ab41435, Abcam), goat anti-CB1R (1:1000, 12,640 S, Cell Signaling Technology), and rabbit anti-synaptophysin (1:1000, 91,954 S, Cell Signaling Technology), rabbit anti-PSD-95 (1:1000, ab238314, Abcam), rabbit anti-β-Tubulin (1:1000, DF7957, Affinity Bioscience) and Na-K ATP (1:1000, ab254025, Abcam). The cut membranes were incubated with primary antibodies at 4℃ overnight and then incubated with a secondary anti-rabbit

(1:10000, ab205718, Abcam) for 2 h at room temperature. The protein contents were revealed with chemiluminescence substrate (A38554, ThermoFisher) and illustrated by the ChemiDoc™ MP imaging system (Bio-Rad). Relative protein expression was quantified using ImageJ (National Institutes of Health) and normalized against the reference proteins. It is noteworthy that sometimes one membrane was treated with stripping and reprobing to visualize different target proteins by incubating with different antibodies.

Locally CB1R Knock-Out

The AAV-CaMKII-Cre-mCherry vector was purchased from BrainVTA (Wuhan, China). The AAV (volume, 200 nl; titer, 1×10^{13}) was stereotactically injected into the right hippocampus of CB1R-flox$^{+/+}$ mice. The injection coordination is AP 1.0 mm, ML 1.5 mm, and DV 2 mm, refer to bregma. To validate the viral infection efficiency, fluorescence labeling and western blotting were performed 4 weeks after injection, as shown in Figure S4.

Cannula Implantation

Surgical cannula implantation was performed to set up a locally acute or chronic drug application route. Briefly, a guide cannula (O.D. 0.20 mm; I.D. 0.16 mm; RWD Apparatus) was implanted over the hippocampal CA1 area (AP, -1.70 mm; ML, 1.25 mm; DV, 1.4 mm) of experimental animals. A dummy cannula (O.D. 0.15 mm; RWD Apparatus) was inserted into the guide cannula to avoid clogging. All implantation locations were verified.

Drug Administration

Gas was diluted in saline to a final 25 mg/ml concentration. To deliver the agent rapidly and accurately, while maintaining high bioavailability, intravenous injection was utilized [43]. Intravenous Gas administration started 28 days after MCAO manipulation, once daily for 7 consecutive days. For the positive control group, we administered 20 mg/kg of fluoxetine intraperitoneally once daily for 7 days to stressed MCAO mice. A PKA inhibitor H89 (HY-15,979, Medchem Express) was dissolved in saline at a concentration of 25 mg/ml and was intraperitoneally injected 30 min before Gas administration. A RhoA agonist U46619 (HY-108,566, Medchem Express) was dissolved in DMSO at a 5 ug/ul concentration. It was microinjected into the right lateral cerebral ventricle through an implanted cannula with a total 2 uL volume. The dose was selected based on a previous study [44]. A Hamilton syringe is connected to the cannula through a polyethylene tube. The injection speed was limited to 1ul in 2 min. The effect of H89 and U46619 was validated by western blotting, as shown in Figure S5.

TTC Staining

The evaluation of infarct volume was conducted 7 days following the MCAO surgery employing TTC staining (103,126, MP Biomedicals). Anesthetized mice were decapitated, and the brains were rapidly removed from the skull and affixed in mouse brain matrix slicers. Subsequently, the brains underwent brief freezing at -20 °C for 15 min before being segmented into 1-mm-thick coronal slices. These sections were then subjected to staining with 2% TTC for 15 min. Regions lacking red staining served as indicators of infarcted tissues.

Laser Speckle Contrast Imaging

To assess cerebral cortical blood flow (CBF) during the MCAO procedure, anesthetized mice were randomly positioned in a prone orientation on a thermostatic mouse plate to facilitate cerebral cortical blood flow monitoring bilaterally via laser speckle contrast imaging (LSCI). The skin and mucous membrane of the head were carefully separated to fully expose the skull. The LSCI system was then focused on the mouse skull to obtain a clear color map. Normal saline was applied to the skull to maintain a moist environment. Baseline cortical blood flow measurements were obtained before modeling, followed by assessments at 5 min post-ischemia and 5 min post-reperfusion. Continuous monitoring was conducted for 15–20 s. CBF within the territory supplied by the right middle cerebral artery was analyzed. A reduction of 80% in CBF followed by a recovery of 70% in this region was indicative of successful MCAO induction.

Golgi Staining

Golgi-Cox staining was performed with NovaultraTM Golgi-Cox Stain Kit (IHC World). Briefly, one day after the last behavioral test, anesthetized mice were decapitated, and the brains were rapidly removed from the skull. Each fresh brain tissue was immersed in Golgi-Cox solution and stored at room temperature for 7 days. The brain tissue was then cut into 100-um thick sections with a vibratome (Leica VT1200 S, Leica Biosystems). The section was washed with distilled water (3 times, 5 min each) and dehydrated with 50% alcohol. The section was ammoniated using 25% ammonia and then washed with distilled water (3 times, 5 min each). The staining was processed with 5% sodium thiosulfate in the dark (10 min). The stained section was washed with distilled water (3 times, 5 min each), followed by PBS wash (3 times, 5 min each). The section was then mounted and air-dried for 1 h. Dehydration was performed in sequence in 50%, 70%, 80%, and 90% ethanol for 5 min each, then in 100% ethanol twice for 10 min each. The slides were then cleared with xylene before coverslipped with permount.

Analysis of Dendritic Complexity

The CA1 neurons from the right hippocampus were analyzed. Neurons meeting the following requirements were chosen to evaluate dendritic complexity: no broken branches, cell body located within CA1, and branches separated from the neighboring neurons. Five randomly distributed neurons from each section in each animal were visualized and analyzed. Dendrites were quantitatively measured using Sholl's concentric circle algorithm for each selected neuron. The intersections were measured at different radial intervals from neuronal soma. Values were averaged for each mouse, and the average value per group was calculated and expressed as mean ± SD.

Analysis of Spine Density

Dendritic spine density was evaluated in the CA1 of the right hippocampus. Dendritic spine distribution analysis was only processed on samples with unbranched, continuously stained, contiguous dendritic segments. Bright-field images of Golgi-impregnated neuronal dendrites from the hippocampal CA1 area were captured with an Olympus DP72 digital camera mounted on an Olympus BX51 microscope (100x oil objective). To calculate spine density, we selected two third-stage branches with a length greater than 30 µm from five randomly distributed neurons in three brain sections of each animal and performed the following analysis. In total, 10 tertiary branches per mouse were counted, and the spine density was evaluated as the average number of spines per 10-µm dendritic segment. Values were averaged per mouse, and the average value per group was calculated and expressed as mean ± SD. The spine density was calculated using ImageJ.

RhoA Activity Assay

RhoA activity was measured using G-LISA Activation Assay Kits (Cytoskeleton). After euthanasia with isoflurane, the mice were killed by decapitation, and the hippocampus tissue was dissected on ice. The tissue samples were then lysed using lysis buffer for 15 min on ice. The lysate was centrifuged at 10,000 × g for 1 min at 4ºC. Supernatants were aliquoted, snap-frozen, and stored at -80ºC. Protein concentrations were measured by a BCA protein assay kit (Beyotime), and the RhoA activity was assessed following the manufacturer's instructions [45].

Statistical Analysis

Statistical analyses were performed using GraphPad Prism 12.0 software. Student's *t*-tests were utilized to compare the differences between two independent groups. One-way ANOVA following Tukey post hoc comparison was performed for multiple groups. Two-way repeated measures ANOVA analysis was used to assess differences between multiple groups in the behavioral tests. All data were presented as the mean ± standard deviation (SD). $p<0.05$ was considered statistically significant.

Results

Gas Treatment Ameliorated Depressive-Like Behaviors in PSD Mice

To confirm the validity of the animal model of PSD, we subjected 8-week-old mice to a 60-minute MCAO, followed by a three-week daily treatment of 3-hour spatial restraint stress for one week after surgical recovery. Subsequently, mice received either saline or Gas administration for another week (Fig. 1A). Motor activity patterns remained consistent between the two groups (Fig. S1D-F). We then conducted a battery of behavioral tests, including the sucrose preference test (SPT), tail suspension test (TST), and forced swim test (FST).

Consistent with previous findings [39], the combination of MCAO and repeated spatial restraint stress induced robust depressive-like behaviors in wild type (WT) animals. In the SPT, sucrose consumption significantly decreased in the saline group compared to the sham group (56.47 ± 5.57% vs. 79.91 ± 13.92%, saline vs. Sham, $p<0.001$, Fig. 1B); In the TST and FST, immobility time of saline-treated stressed MCAO mice was significantly longer than the sham group (In TST, 191.87 ± 24.92s vs. 85.31 ± 13.92s, Saline vs. Sham, $p<0.001$, Fig. 1C; In FST, 204.98 ± 22.81s vs. 104.40 ± 13.04s, Saline vs. Sham, $p<0.001$, Fig. 1D). We did not observe any notable differences in these behaviors between the sham and Sham + SRS groups, indicating that SRS alone could not induce depressive-like behavior.

Next, we investigated whether Gas treatment could alleviate depressive-like behaviors in PSD mice in a dose-dependent manner. The results showed that while 50 mg/kg of Gas treatment did not normalize stress-induced depressive-like behaviors in MCAO mice, both 100 mg/kg and 200 mg/kg Gas treatments significantly increased total sucrose consumption in the SPT (68.03 ± 8.09% vs. 56.47 ± 5.57%, Gas-100 vs. saline, $p<0.01$, 72.40 ± 9.42% vs. 56.47 ± 5.57%, Gas-200 vs. saline, $p<0.01$, Fig. 1B), reduced immobility times in the TST (140.76 ± 20.73s vs. 191.87 ± 24.92s, Gas-100 vs. saline, $p<0.01$, 125.61 ± 11.92s vs. 191.87 ± 24.92s, Gas-200 vs. saline, $p<0.01$, Fig. 1C) and FST (148.01 ± 24.73s vs. 204.98 ± 22.81s, Gas-100 vs. saline, $p<0.01$, 132.85 ± 18.93 s vs. 204.98 ± 22.81s, Gas-200 vs. saline, $p<0.01$, Fig. 1D) compared to the saline group. Notably, there was no comparable difference

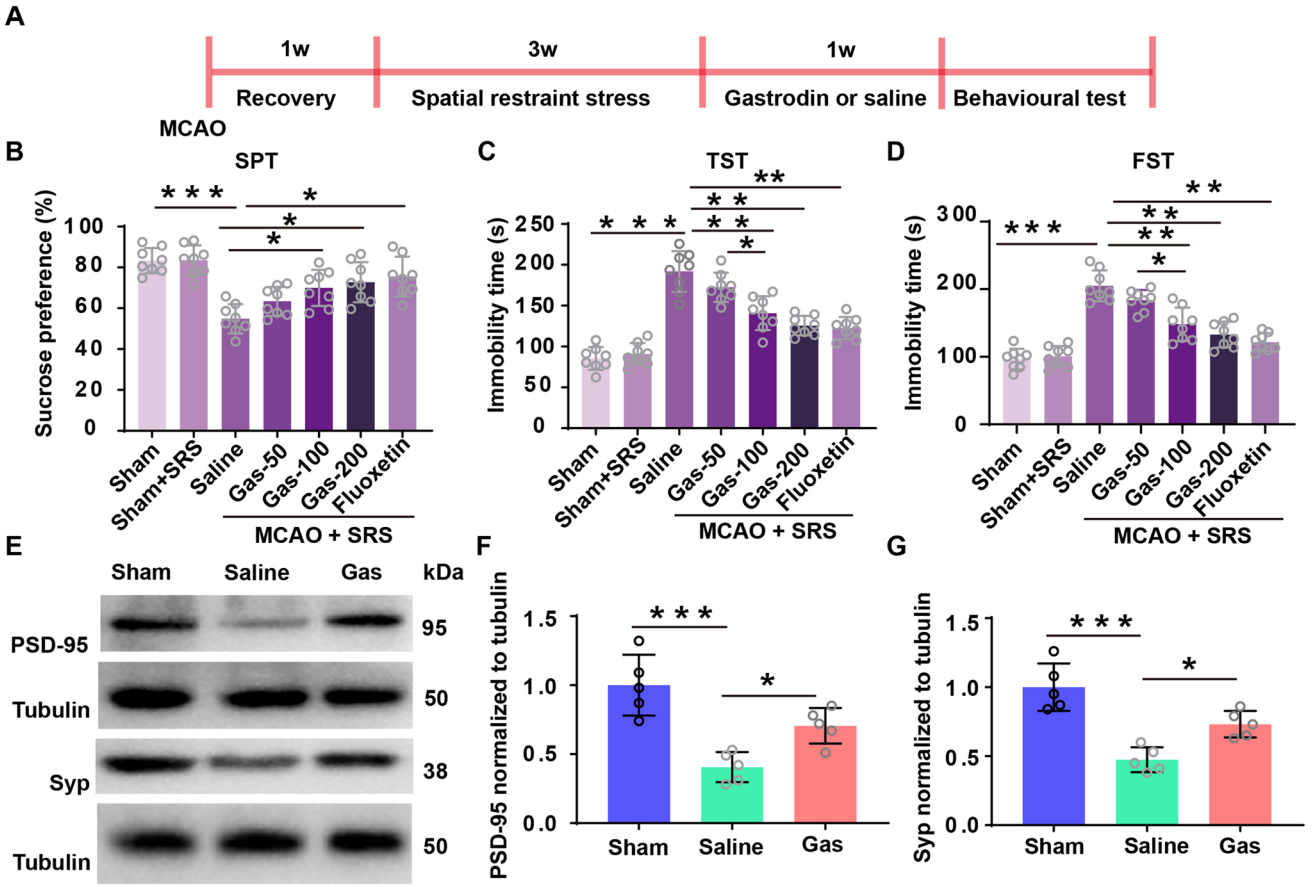

Fig. 1 Gastrodin reverses depressive-like behaviors and expression deficiency of synaptic-associated proteins in PSD mice.**A,** Schematic depicting experimental procedure. Animals were allowed for a 1-week recovery after MCAO manipulation, followed by a 3-week spatial restraint stress induction and 1-week Gas at different dosages or vehicle treatment, and behavioral tests were performed afterward. **B,** Sucrose preference ratio of mice among Sham, Sham + SRS, Saline, Gas-50, Gas-100, Gas-200, and Fluoxetine groups after 1 week of Gas administration. **C, D,** Quantification of performance on TST (**C**) and FST (**D**) showing that the immobility durations were reversed by Gas treatment. **E,** Representative images showing western blotting of PSD-95 and Syp proteins level in hippocampal tissue extracts of sham mice and saline-, Gas-treated PSD mice.**F,** Quantification of PSD-95 protein level. **G,** Quantification of Syp protein level. Data were presented as mean ± SD and analyzed using one-way ANOVA followed by Tukey's post hoc test. $^{*}p < 0.05$, $^{**}p < 0.01$,$^{***}p < 0.001$, $n = 8$ (when detecting depressive-like behaviors) and n=5 (when testing synaptic associated protein) mice per group

between the effects of the 100 mg/kg and 200 mg/kg Gas treatments (For SPT, 68.03 ± 8.09% vs. 72.40 ± 9.42%, Gas-100 vs. Gas-200, p>0.05; For TST, 140.76 ± 20.73s vs. 125.61 ± 11.92s, Gas-100 vs. Gas-200, p>0.05, For FST, 148.01 ± 24.73s vs. 132.85 ± 18.93 s, Gas-100 vs. Gas-200, p>0.05, Fig. 1D). Additionally, there was no significant difference in Gas treatment at 100 mg/kg when compared to the Fluoxetine group (For SPT, 68.03 ± 8.09% vs. 75.5 ± 9.67%, Gas-100 vs. Fluoxetine, p>0.05, Fig. 1B; For TST, 140.76 ± 20.73s vs. 122.62 ± 13.58s, Gas-100 vs. Fluoxetine, p>0.05, Fig. 1C; For FST, 148.01 ± 24.73s vs. 123.73 ± 14.21s, Gas-100 vs. Fluoxetine, p>0.05, Fig. 1D). Having observed the effective reduction of depressive-like behaviors through the administration of 100 mg/kg Gas, and noting the similar efficacy between 100 mg/kg and 200 mg/kg dosages, we have decided to continue using this dosage for further investigations, taking into account potential side effects, individual tolerance, and cost-effectiveness [46].

To further elucidate the time-dependent effect of Gas treatment, we conducted experiments to compare the impact of Gas treatment on depressive-like behaviors in PSD mice over both 1-week and 2-week administration periods. Our findings revealed that although there was a noticeable trend towards increased sucrose consumption (68.03 ± 8.09% vs. 75.98 ± 6.86%, Gas-1w vs. Gas-2w, p>0.05, Fig. S2A) and reduced immobility time in the TST (140.76 ± 20.73s vs. 123.01 ± 12.12 s, Gas-1w vs. Gas-2w, p>0.05, Fig. S2B) and FST (148.01 ± 24.73s vs. 128.00 ± 21.11 s, Gas-1w vs.Gas-2w, p>0.05, Fig. S2C) tests with 2-week Gas administration, the overall efficacy in mitigating depressive-like behaviors was comparable between the two experimental conditions.

Given the involvement of impaired synaptic plasticity and synaptogenesis in the pathomechanism of both stroke and depression, we next aim to identify the effect of Gas on these processes in hippocampal neurons. We examined the expression levels of post-synaptic density protein 95 (PSD-95) and Synaptophysin (Syp) in the hippocampus (Fig. 1E). The data revealed lower expression of PSD-95 (0.41 ± 0.09 vs. 1.0 ± 0.21, saline vs. sham, $p<0.001$, Fig. 1F) and Syp (0.47 ± 0.09 vs. 1.0 ± 0.16, saline vs. sham, $p<0.05$, Fig. 1G) in the saline-treated group compared to the sham group. Gas intervention markedly reversed this reduction of PSD-95 (0.73 ± 0.09 vs. 0.41 ± 0.09, Gas vs. saline, $p<0.001$) and Syp (0.78 ± 0.13 vs. 0.47 ± 0.09, Gas vs. saline, $p<0.05$), indicating its potential in restoring synaptic protein expression. Golgi-staining results further demonstrated a decrease in dendrite complexity and dendritic spine density in the hippocampal CA1 region of saline-treated PSD animals compared to the Sham group. In contrast, Gas application increased dendrite complexity and dendritic spine density (Fig. 2A-D), suggesting that the anti-PSD effect of Gas involves the restoration of neuroplasticity and synaptogenesis, crucial contributing factors to PSD pathophysiology.

Gas Application Reversed the Impaired CB1R Expression on the Presynaptic GABAergic Terminal in CA1 of PSD Mice

The identification of potential downstream targets for Gas has remained elusive. Recent reports have suggested the involvement of the cannabinoid system in mediating the development of PSD [47, 48]. To explore the potential relationship between Gas and cannabinoid signaling pathways, we initiated molecular docking studies to predict the binding targets of Gas with CB1R.

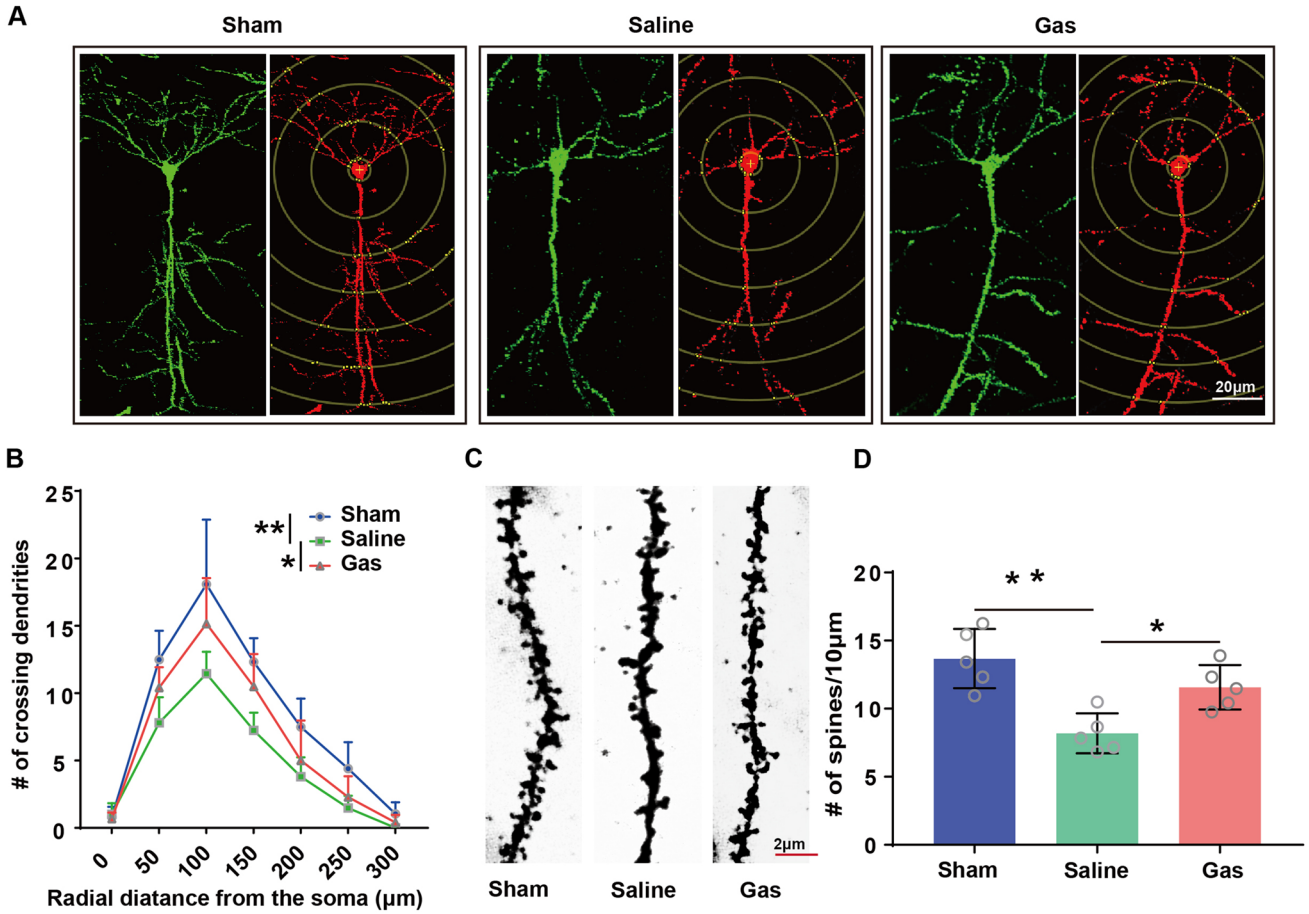

Fig. 2 The effect of Gas on dendritic complexity and spine density. **A,** Representative images showing a typical single Golgi-impregnated neuron in CA1of sham (left) mice and saline- (middle), Gas-treated (right) PSD mice. **B,** Quantification of the mean number of Sholl intersection profiles in CA1 of sham mice and saline-, Gas-treated PSD mice. **C,** Representative photomicrographs showing typical dendritic spine structure of CA1 neurons in sham (left) mice and saline- (middle), Gas-treated (right) PSD mice. **D,** Quantification of dendritic spine density of CA1 neurons in sham and saline-, Gas-treated PSD mice. Data were presented as mean ± SD and analyzed using one-way ANOVA followed by Tukey's post hoc test. $^{*}p < 0.05$, $^{**}p < 0.01$, $n = 5$ mice per group

The molecular docking results demonstrated a robust binding interaction between Gas and CB1R, with a binding energy of -7.54 kcal/mol. The active amino acid residues in CB1R, including YRP-279, THR-197, SER-383, PHE- 268, PHE-379, PHE-174, PHE-170, and PHE-200, were identified as potential interaction sites with Gas. Additionally, Gas exhibited significant hydrophobic interactions with PHE-268, PHE-379, PHE-174, PHE-170, and PHE-200 in CB1R. The benzene ring of Gas formed pi-conjugated interactions with TRP-279, contributing to the stabilization of these small molecules (Fig. 3A, B). These interactions collectively promote the formation of stable complexes between Gas and CB1R.

To validate the relationship between Gas and CB1R, we employed immunofluorescence and WB methods to assess CB1R expression in the CA1 region of the hippocampus. Results indicated a decrease in CB1R expression in the saline-treated stressed MCAO mice (Saline group) compared to the Sham group (0.49 ± 0.16 vs. 1.0 ± 0.15, Saline vs. Sham, $p<0.001$, Fig. 3C), while Gas treatment did not affect the overall expression of CB1R (0.52 ± 0.11 vs. 0.49 ± 0.16, Gas vs. Saline, $p>0.05$, Fig. 3C, Fig. S3). However, examination of CB1R levels on the membrane, a determinant of CB1R activity, revealed a decrease in the Saline group (0.42 ± 0.07 vs. 1.0 ± 0.11, Saline vs. Sham, $p<0.001$, Fig. 3D) and an increase with Gas administration (0.61 ± 0.10 vs. 0.42 ± 0.07, Gas vs. Saline, $p<0.01$, Fig. 3D). This suggests that CB1R activity decreased during PSD development, as the level membrane-bound CB1R reflects its biological activity [49].

CB1R is extensively expressed at the presynaptic site, exerting an inhibitory role in regulating retrograde signaling-mediated neurotransmission. Previous studies show that CB1Rs are primarily located at GABAergic terminals in the hippocampus to control GABA release [50, 51]. Further investigation into the subcellular distribution of CB1R expression, co-staining with presynaptic GABAergic neuronal marker (vGAT) or presynaptic glutamatergic neuronal marker (vGlut1), revealed a reduction in CB1R expression mainly at GABAergic terminals in saline-treated stressed MCAO mice (Fig. 3E, F). In contrast, CB1R expression at glutamatergic terminals remained intact under these experimental conditions (Fig. 3H-G). Gas application reversed the impaired CB1R expression at GABAergic terminals (Fig. 3E, F), implicating the involvement of CB1R at these sites in Gas's anti-PSD effect by modulating GABAergic neurotransmission.

The Anti-PSD Effect of Gas is Dependent on CB1R Expressed in CA1 Pyramidal Neurons

We further sought to determine whether the anti-PSD effect of Gas is dependent on the expression of CB1R in CA1 pyramidal neurons. To this end, we assessed depressive-like behaviors, dendritic spine density, dendrite complexity, and synaptic plasticity-related proteins in stressed MCAO mice with local CB1R depletion in the hippocampus. The impact of Gas on the sucrose preference test ($58.06 \pm 7.33\%$ vs. $70.05 \pm 10.11\%$, Gas + Cre vs. Gas + mCherry, $p<0.05$, Fig. 4A), immobility times in the TST (191.46 ± 24.39 s vs. 144.73 ± 21.62 s, Gas + Cre vs. Gas + mCherry, $p<0.05$, Fig. 4B) and immobility times in the FST (196.21 ± 34.20 s vs. 151.86 ± 23.43 s, Gas + Cre vs. Gas + mCherry, $p<0.01$, Fig. 4C) showed partially abrogation when we locally knocked out CB1R in hippocampal CA1 region. Concurrently, local depletion of CB1R diminished the effect of Gas on PSD-95 (0.54 ± 0.10 s vs. 0.966 ± 0.13, Gas + Cre vs. Gas + mCherry, $p<0.05$, Fig. 4D, E) and Syp expression (0.48 ± 0.10 vs. 1.02 ± 0.14, Gas + Cre vs. Gas + mCherry, $p<0.05$, Fig. 4D, F). Moreover, local knockout of CB1R attenuated the effect of Gas on increasing dendrite complexity (Fig. 5A, B) and dendritic spine density (Fig.5C, D). Importantly, no statistical difference was observed between the Gas + mCherry group and the Gas group for the aforementioned indexes. These findings collectively emphasize the functional significance of CB1R expression in CA1 pyramidal neurons in mediating the anti-PSD effect of Gas.

Gas Application Impacted the PKA/RhoA Signaling Pathway Through CB1R

As disrupted synaptogenesis and alterations in synaptic plasticity-related proteins contribute to the development of PSD, it implicates a role in impaired cytoskeletal integrity in this progression. Recent reports have emphasized the involvement of the PKA/RhoA signal pathway, governing cytoskeletal dynamics and synaptogenesis, in the development of PSD, hinting a potential interaction between the PKA/RhoA pathway and CB1Rs [33, 52]. Evidence has shown that PKA, regulating cellular membrane structural plasticity through RhoA, phosphorylates RhoA on Ser188, leading to decreased RhoA activity [35, 53]. We sought to investigate whether the PKA/RhoA signal pathway contributes to the anti-PSD effect of Gas.

To this end, we analyzed the expression levels of p-PKA, PKA, p-RhoA, and RhoA. Gas application significantly increased the expression of p-PKA (0.72 ± 0.10 vs. 0.33 ± 0.10, Gas vs. saline, $p<0.05$, Fig. 6A, B). However, this effect on p-PKA was less pronounced when CB1R was locally deleted in the CA1 region of the hippocampus (0.43 ± 0.06 vs. 0.78 ± 0.10, Gas + Cre vs. Gas + mCherry, $p<0.05$, Fig. 6A, B). Meanwhile, the content of PKA did not exhibit significant changes (Fig. 6A, C). Additionally, Gas up-regulated the expression of p(ser188)-RhoA(indicating RhoA inactivation [33]) (0.62 ± 0.11 vs. 0.24 ± 0.08, Gas vs. saline, $p<0.01$, Fig. 6A, D), while

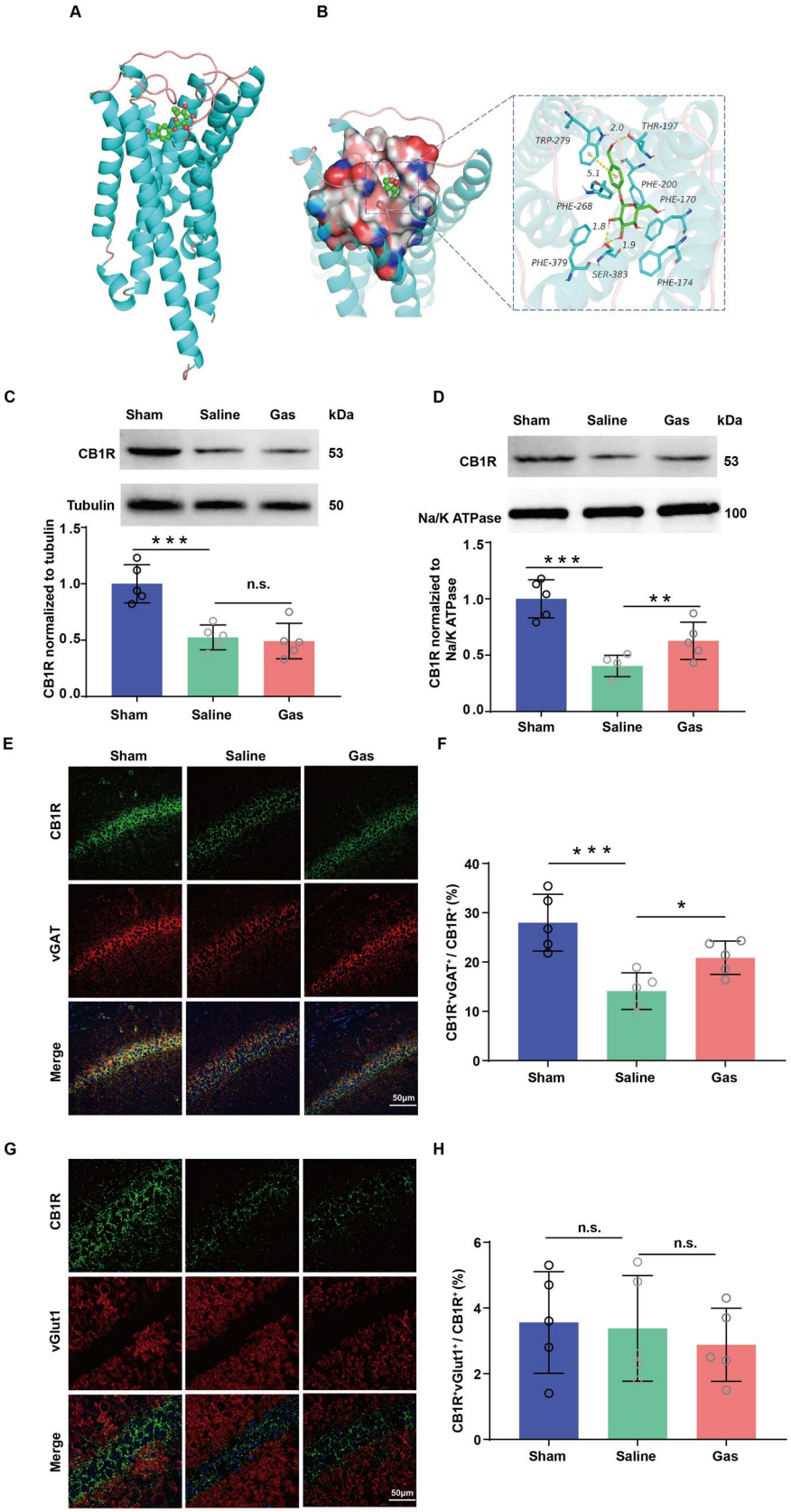

Fig. 3 The effect of Gas on CB1R expression in the hippocampal CA1 of PSD mice. **A, B,** Docking, and binding diagram of Gas and CB1R molecules. (**A**) shows the 3D interaction patterns of Gas and CB1R molecules. (**B**) shows the 3D docking diagram of Gas and CB1R molecules. **C,** Quantification of the total CB1R protein levels in sham mice and saline-. **D,** Quantification of the membrane CB1R protein levels in sham mice and saline-, Gas-treated PSD mice. **E,** Representative images showing co-localization of CB1R and vGAT in hippocampal CA1 of sham mice and saline-, Gas-treated PSD mice. **F,** Quantification of the ratio of CB1R and vGAT double positive to CB1R in sham mice and saline-, Gas-treated PSD mice. **G,** Representative images showing co-localization of CB1R and vGlut1 in hippocampal CA1 of sham mice and saline-, Gas-treated PSD mice. **H,** Quantification of the ratio of CB1R and vGlut1 double positive to CB1R in sham mice and saline-, Gas-treated PSD mice. Data were presented as mean ± SD and analyzed using one-way ANOVA followed by Tukey's post hoc test. *$p < 0.05$, **$p < 0.01$, ***$p < 0.001$, n.s. represents no significance, n=5 mice per group

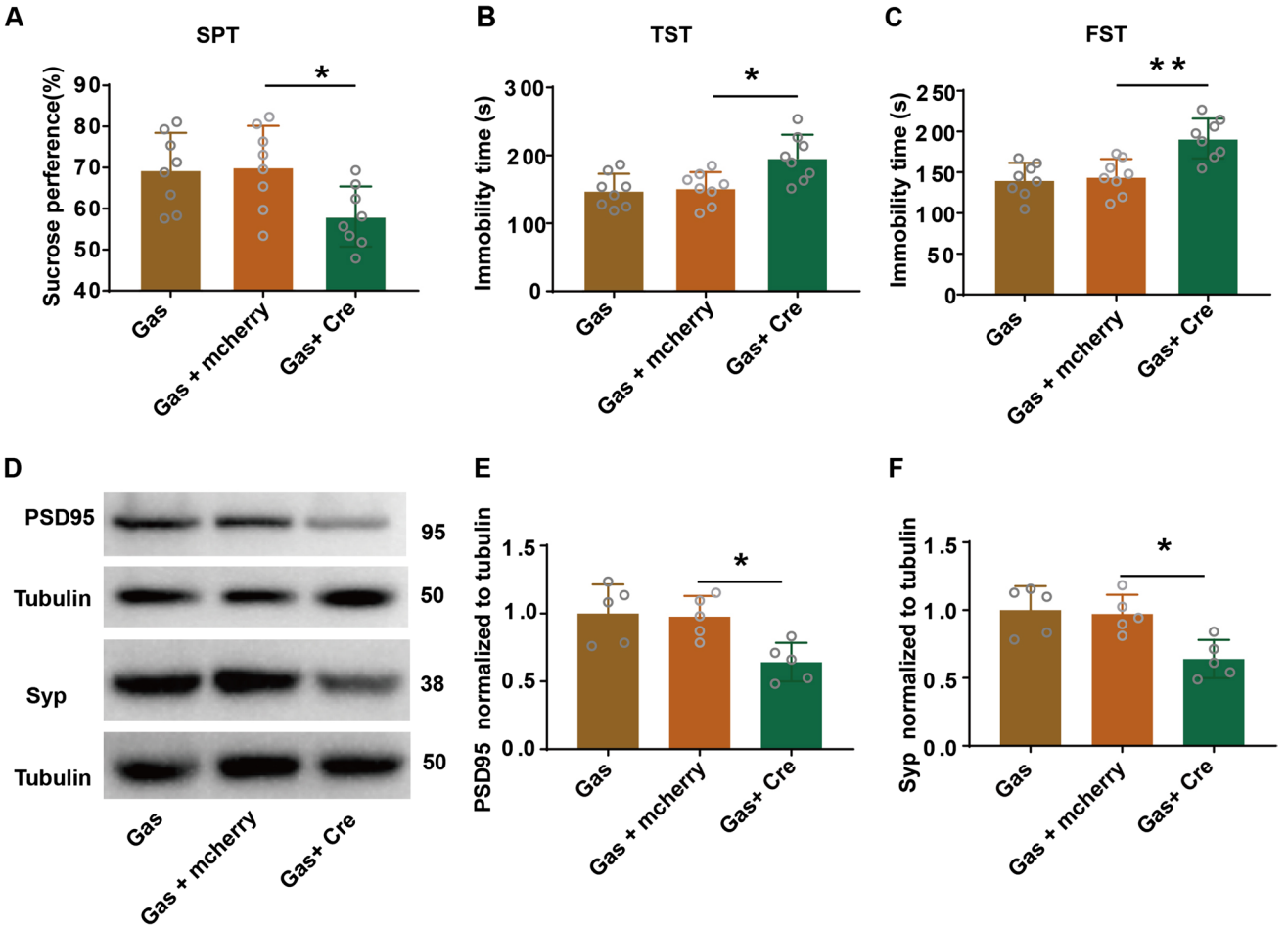

Fig. 4 CB1R participates in the exertion of the functional role of Gas in regulating depressive-like behavioral performance and synaptic-associated protein expression. **A,** Sucrose preference ratio of mice among Gas, Gas + mCherry, and Gas + Cre groups of PSD CB1R-flox mice after 1 week of Gas administration. **B, C,** Quantification of performance on TST (**B**) and FST (**C**) showing that the anti-depression effect of Gas manifested as reduced immobility durations were blocked by CB1R depletion. **D,** Representative images showing western blotting of PSD-95 and Syp proteins level in hippocampal tissue extracts of Gas, Gas + mCherry, and Gas + Cre groups of PSD CB1R-flox mice. **E,** Quantification of PSD-95 protein level. **F,** Quantification of Syp protein level. Data were presented as mean ± SD and analyzed by one-way ANOVA followed by Tukey's post hoc test. *$p < 0.05$, **$p < 0.01$, $n = 8$ (when detecting depressive-like behaviors) and n=5 (when testing synaptic associated protein) mice per group

local knockout of CB1R in the hippocampus partially reversed this effect (0.30 ± 0.08 vs. 0.75 ± 0.10, Gas + Cre vs. Gas + mCherry, $p<0.05$, Fig. 6A, D). No notable difference was observed between the Gas group and Gas + mCherry group (Fig. 6A, D), and the total expression level of RhoA among those experimental groups remained relatively unchanged (Fig. 6A, E).

Further assessment of RhoA activity using G-LISA revealed that Gas inhibited the activity of RhoA (1.83 ± 0.11 vs. 2.56 ± 0.53, Gas vs. saline, $p<0.05$, Fig. 6F). However, local depletion of CB1R in the hippocampus when compared with the Gas + mCherry group, abolished the effect of Gas on RhoA activity (2.63 ± 0.35 vs. 1.87 ± 0.20, Gas + Cre vs. Gas + mCherry, $p<0.05$, Fig. 6F). These results suggest the involvement of the PKA/RhoA signaling pathway in the anti-PSD response induced by Gas and highlight the role of CB1R activation in mediating this neurobiological process.

Inhibition of PKA or Activation of RhoA Reversed the Anti-PSD Effect of Gas

Next, to assess the involvement of the PKA/RhoA pathway in the anti-PSD effect of Gas, we administrated the PKA inhibitor H89 (intraperitoneally) and the RhoA activator U46619 (intracerebroventricularly) in PSD mice.

Analyses of depressive-like behaviors, synaptic plasticity-related proteins, dendritic spine density, and dendrite complexity were conducted in the fifth week after the MCAO.

Results indicated that H89 treatment led to a decrease in the consumption of sucrose water (56.21 ± 5.39%

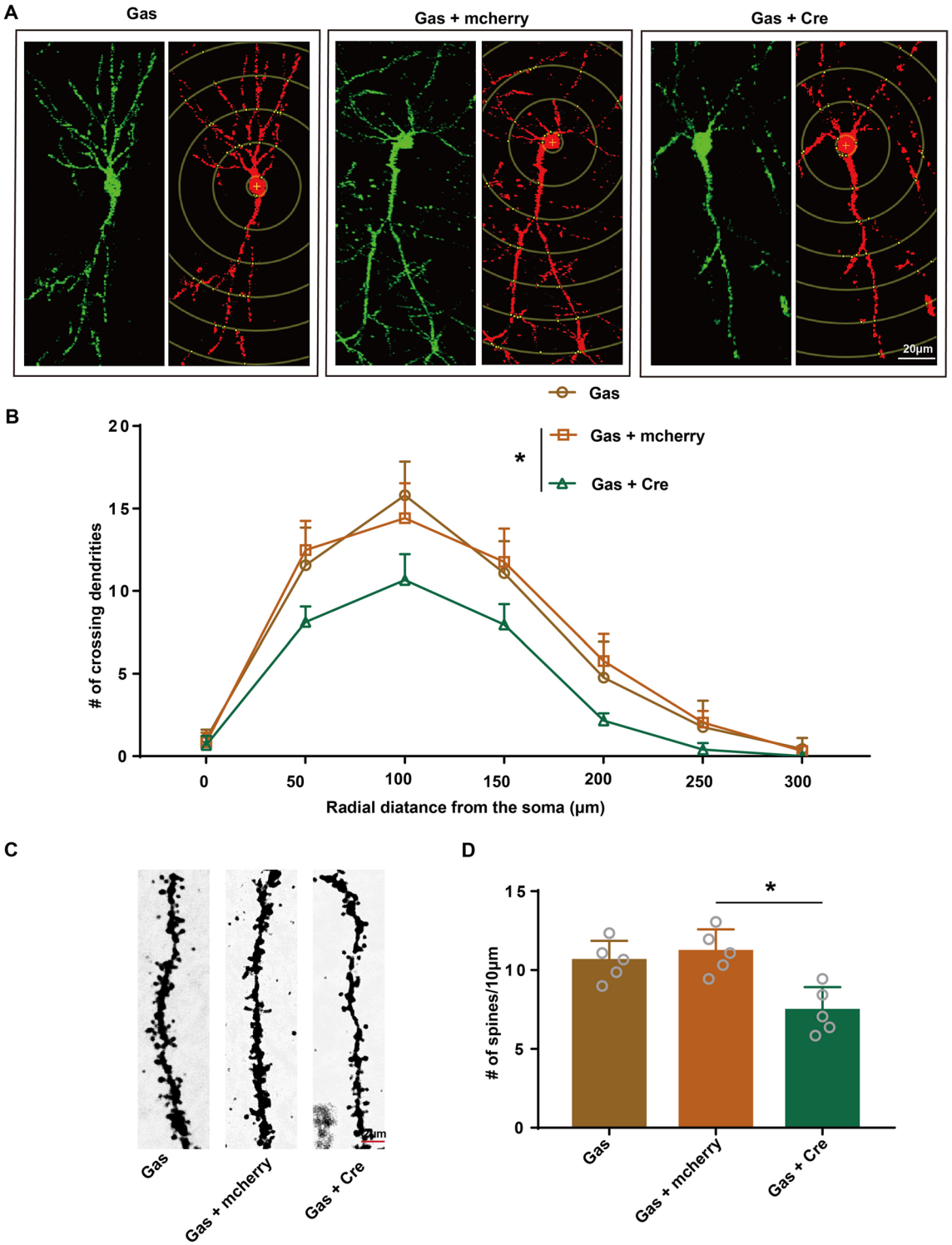

Fig. 5 CB1R participated in the exertion of the functional role of Gas in modulating dendritic complexity and spine density. **A**, Representative images showing a typical single Golgi-impregnated neuron in CA1 of Gas (left), Gas + mCherry (middle), and Gas+ Cre (right) groups of PSD CB1R-flox mice. **B**, Quantification of the mean number of Sholl intersection profiles in CA1 of Gas, Gas + mCherry, and Gas + Cre groups of PSD CB1R-flox mice. **C**, Representative photomicrographs showing typical dendritic spine structure of CA1 neurons in Gas (left), Gas + mCherry (middle), and Gas + Cre (right) groups of PSD CB1R-flox mice. **D**, Quantification of dendritic spine density of CA1 neurons in Gas, Gas + mCherry, and Gas + Cre groups of PSD CB1R-flox mice. Data were presented as mean ± SD and analyzed by one-way ANOVA followed by Tukey's post hoc test. * $p < 0.05$, n=5 mice per group

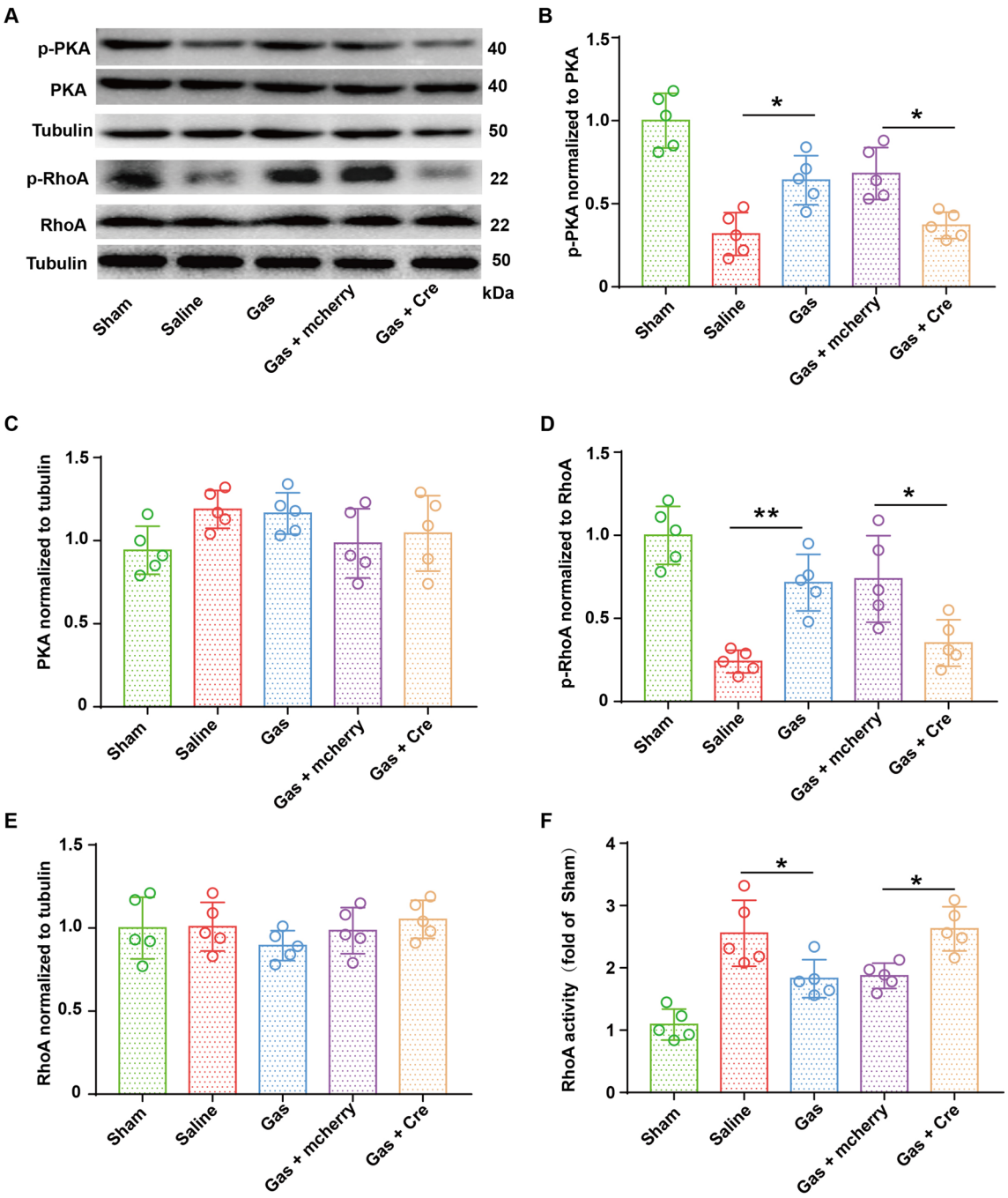

Fig. 6 Gas regulates the PKA/RhoA signaling pathwayin PSD mice through CB1R.**A,** Representative images showing western blotting of PKA, p-PKA,p-RhoA and RhoA proteins level in hippocampal tissue extracts of sham mice, saline-, Gas-treated PSD mice, and Gas + mCherry, Gas + Cre groups of PSD CB1R-flox mice.**B,** Quantification of p-PKA protein level. **C,** Quantification of PKA protein level. **D,** Quantification of p-RhoA protein level. **E,** Quantification of RhoA protein level. **F,** Quantification of activity of RhoA protein. Data were presented as mean ± SD and analyzed by one-way ANOVA followed by Tukey's post hoc test. *$p < 0.05$, **$p < 0.01$, n=5 mice per group

vs. 72.87 ± 7.26%, H89 vs. saline, $p<0.01$, Fig. 7A), an increase in immobility during the TST (193.96 ± 19.86 vs. 139.25 ± 17.45 s, H89 vs. saline, $p<0.001$, Fig. 7B) and FST (179.76 ± 15.44s vs. 131.85 ± 16.97 s, H89 vs. saline, $p<0.001$, Fig. 7C), and a reduction in the expression of PSD-95 (0.44 ± 0.1 vs. 1.0 ± 0.13, H89 vs. saline, $p<0.01$, Fig. 7D, E) and Syp (0.42 ± 0.1 vs. 1.0 ± 0.22, H89 vs. saline, $p<0.01$, Fig. 7D, F) compared to the Gas + saline group. Similarly, activation of the RhoA pathway with U46619 application nullified the Gas-induced increase

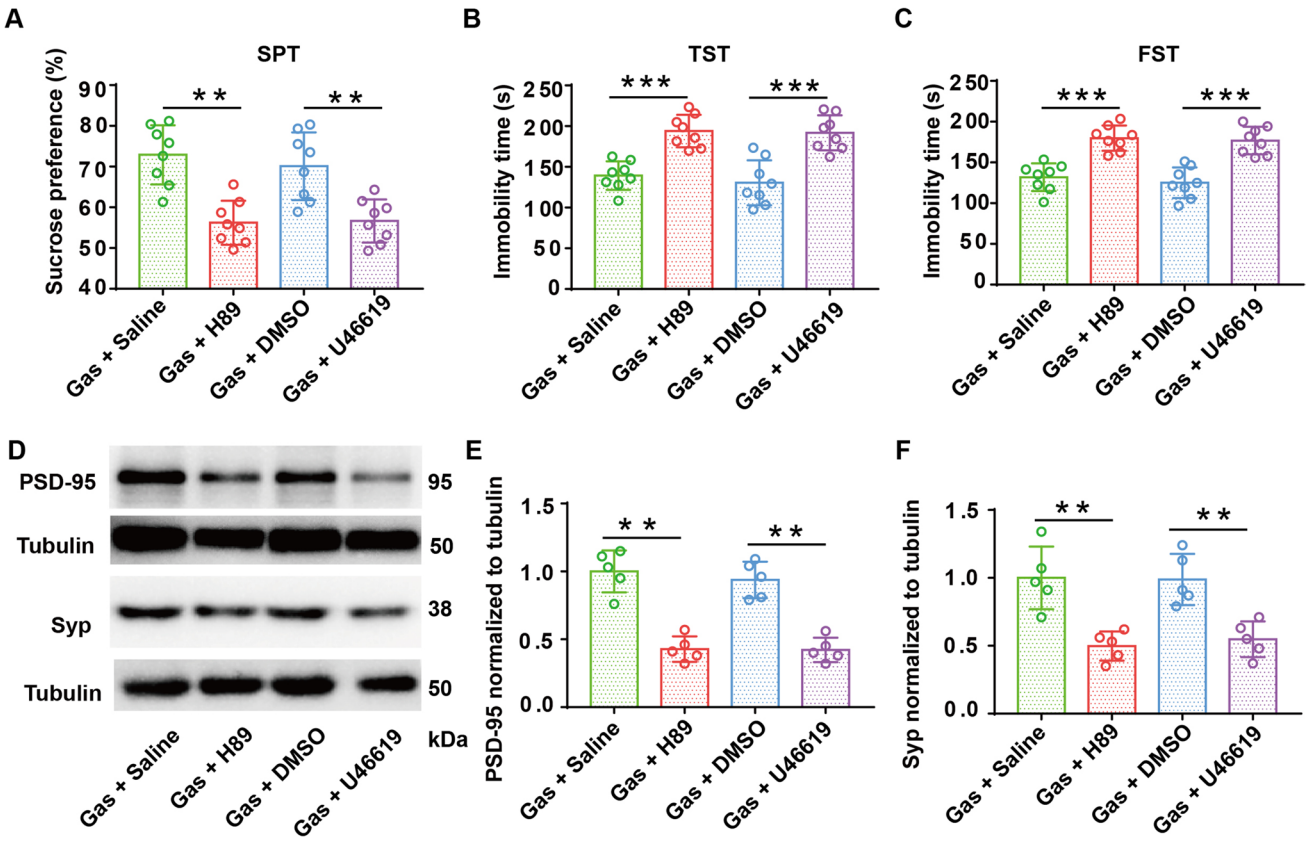

Fig. 7 The effect of Gas on depressive-like behaviors and synaptic associated protein is dependent on the PKA/RhoA signaling pathway. **A,** Sucrose preference ratio of mice among Gas + saline, Gas + H89, Gas + DMSO, and Gas + U46619 groups of PSD mice after one week of Gas administration. **B, C,** Quantification of performance on TST (**B**) and FST (**C**) showing that the anti-depression effect of Gas manifested as reduced immobility durations were blocked by either p-PKA inhibition or p-RhoA activation. **D,** Representative images showing western blotting of PSD-95 and Syp proteins level in hippocampal tissue extracts of Gas + saline, Gas + H89, Gas + DMSO, and Gas+ U46619 groups of PSD mice. **E,** Quantification of PSD-95 protein level. **F,** Quantification of Syp protein level. Data were presented as mean ± SD and analyzed by one-way ANOVA followed by Tukey's post hoc test. $^{**}p < 0.01$, $^{***}p < 0.001$, $n = 8$ (when detecting depressive-like behaviors) and n=5 (when testing synaptic associated protein) mice per group

in sucrose consumption (54.65 ± 5.30% vs. 70.08 ± 8.2%, U46619 vs. DMSO, p<0.01, Fig. 7A), the Gas-induced reduction in immobility during TST (191.78 ± 21.41s vs. 130.45 ± 27.64 s, U46619 vs. DMSO, p<0.001, Fig. 7B) and FST (176.81 ± 16.95 s vs. 125.06 ± 18.86 s, U46619 vs. DMSO, p<0.001, Fig. 7C), and the Gas-induced enhancement of PSD-95 (0.41 ± 0.07 vs. 0.89 ± 0.11, U46619 vs. DMSO, p<0.01, Fig. 7D, E) and Syp expression (0.56 ± 0.12 vs. 1.06 ± 0.16, p<0.01, Fig. 7D, F) compared with the Gas + DMSO group.

Additionally, our data revealed that the H89 application decreased the complexity of dendrites (Fig. 8A, B) and the density of dendritic spines (Fig. 8C, D). Meanwhile, the activation of RhoA with U46619 application counteracted the Gas-induced increase in dendrite complexity (Fig. 8A, B) and dendritic spine density (Fig. 8C, D). These results demonstrated that the anti-PSD effect of Gas relies on the PKA/RhoA signaling pathway, either directly or indirectly, through CB1R activation.

Discussion

Our investigation delved into the behavioral and morphological repercussions of mild brain ischemia in mice and established Gas's functional role in ameliorating the depression-like state in this animal model. Combining spatial restraint stress and MCAO successfully replicated core depressive features after brain ischemia in mice (Fig. 1B-D). We presented evidence suggesting that defects in neuronal synaptic functions and spine morphogenesis in the hippocampus are potential mechanisms of post-stroke depression (PSD). Our data indicated that a one-week administration of Gas effectively reversed depressive-like

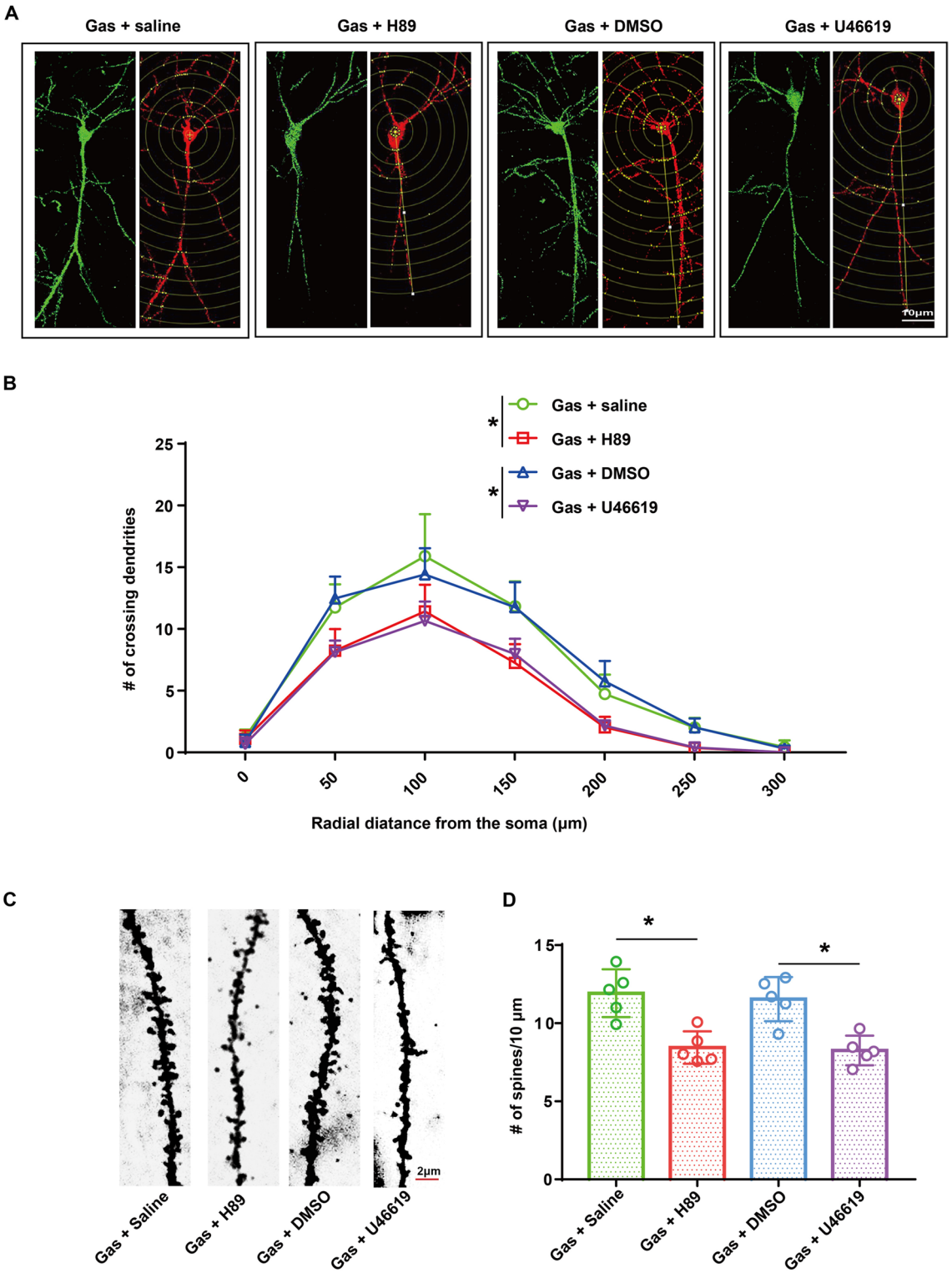

Fig. 8 The effect of Gas on dendritic complexity and spine density is mediated by the PKA /RhoA signaling pathway.**A,** Representative images showing a typical single Golgi-impregnated neuron in CA1 of Gas + saline (left), Gas + H89 (middle left), Gas + DMSO (middle right), and Gas + U46619 (right) groups of PSD mice.**B,** Quantification of the mean number of Sholl intersection profiles in CA1 of Gas + saline, Gas + H89, Gas + DMSO, and Gas + U46619 groups of PSD mice. **C,** Representative photomicrographs showing typical dendritic spine structure of CA1 neurons in Gas + saline (left), Gas + H89 (middle left), Gas + DMSO (middle right), and Gas + U46619 (right) groups of PSD mice. **D,** Quantification of dendritic spine density of CA1 neurons in Gas + saline, Gas + H89, Gas + DMSO, and Gas + U46619 groups of PSD mice.Data were presented as mean ± SD and analyzed by one-way ANOVA followed by Tukey's post hoc test. *$p < 0.05$, n=5 mice per group

behavioral and synaptic deficits. Notably, we identified CB1R as a potential affinity target for Gas to exert its neuroprotective role, subsequently recruiting the PKA/RhoA-related signaling pathway to regulate synaptic transmissions and spine morphogenesis in the hippocampal area. Furthermore, we demonstrated that the anti-PSD effect of Gas was impeded by inhibiting PKA or increasing RhoA activity.

Previous studies have indicated that pharmacological interventions by using conventional antidepressants, such as imipramine, fluoxetine, and citalopram, can effectively attenuate post-stroke depressive-like behaviors in rodents [39, 54, 55]. This aligns with clinical reports demonstrating the positive effects of chronic antidepressant treatment on various stroke outcomes in human patients [4, 56]. Building on the validity of our model, we emphasize the term "post-stroke depressive-like behaviors in mice" to indicate the behavioral changes observed in stressed MCAO mice distinctly. This terminology underscores the relevance of our findings to the specific context of depressive states following ischemic stroke in the murine model. It is noteworthy that the majority of conventional antidepressants have been developed based on the monoaminergic theory, which focuses on the modulation of dopaminergic, serotoninergic, and norepinephrinergic neurotransmission [57]. However, a significant proportion of patients exhibit drug resistance to these conventional antidepressants, indicating the involvement of alternative underlying mechanisms in the pathogenesis of depression [58]. Furthermore, the commonly prescribed first-line antidepressant medications, selective serotonin reuptake inhibitors (SSRIs), are associated with significant side effects [59], underscoring the need for novel therapeutic targets and gentler treatment options. Our study has identified a distinct molecular pathway that may contribute to the development of post-stroke depression. Notably, this pathway serves as a functional target of Gas, an active component extracted from medicinal herbs. Considering previous reports highlighting Gas's neuroprotective properties and fewer side effects [7, 16], it is conceivable that Gas could offer significant value as an adjunctive or supplementary treatment option within the spectrum of antidepressant medications.

Clinical studies highlight that stroke is a significant risk factor for depression, and reciprocally, depression is independently associated with stroke, suggesting shared etiological mechanisms [2]. The observed overlap is further substantiated by the fact that antidepressants not only expedite recovery from stroke but also contribute to the amelioration of post-stroke depression, underscoring common pathophysiology and therapeutic targets for depression and stroke [3, 4]. Our study reinforces this connection by demonstrating that Gas effectively alleviates depressive-like behaviors in PSD mice. These findings align with prior reports indicating the potential benefits of Gas administration in the context of ischemic stroke [9, 16, 60]. The positive impact of Gas on both depressive symptoms and ischemic outcomes underscores its potential as a multifaceted therapeutic intervention for conditions where depression and stroke coalesce.

The escalating use of cannabis for both medical and recreational purposes has drawn attention to its potential impact on mental health, with anxiety and depression being frequently cited motivations [21, 24, 61]. The close interconnection between stress-related mental disorders and the cannabinoid system is underscored by the expression of CB1R in brain regions linked to stress and cognition, such as the prefrontal cortex, amygdala, and hippocampus in humans [20, 56]. Recent research has unveiled intricate dynamics within the cannabinoid system, particularly in response to chronic stress. Studies indicate that CB1R downregulation in specific neural circuits can enhance stress susceptibility, while CB1R agonists exert an antidepressant-like effect, suggesting a pivotal role of CB1R in stress-related disorders [25]. Notably, reports showed that CB1R expression decreases in the ventral medial hypothalamus, and activated CB1R attenuates depressive-like behaviors in PSD rats [27]. The neuroprotective role of CB1R is further supported by studies demonstrating more severe ischemia-induced brain injury in CB1R knockout mice compared to wild-type mice [47, 62].

In alignment with these findings, our data reveals a reduction in hippocampal neuronal membrane CB1R expression associated with post-stroke depressive-like behaviors in rodents. Interestingly, Gas administration reverses this reduction, suggesting a nuanced interplay between CB1R and the Gas-involved signaling pathway. The extensive expression of CB1R in GABAergic terminals in the hippocampus, known for its critical role in neuroprotection through modulating glutamate release [63], prompts the hypothesis that diminished CB1R expression at these terminals amplifies inhibitory tone, resulting in reduced glutamatergic neurotransmission. We proposed that ischemic stroke leads to long-term genetic changes, including a reduction in CB1R expression on presynaptic GABAergic terminals. This reduction alters the balance between excitatory and inhibitory signaling in the hippocampus, resulting in impaired expression of synaptic proteins. We hypothesized that this alteration is mediated by disrupted CB1R-related presynaptic inhibition and may contribute to the development of depressive-like behaviors in stressed MCAO mice. Exploring the molecular interaction between Gas and CB1R, our study employed a computer-assisted molecular docking algorithm, revealing a robust binding affinity. However, the complexity of CB1R-participated non-canonical signaling pathways, involving interactions with dopamine type-2 receptors, adenosine receptors, and orexin receptors, introduces intricacies [64, 65]. The possibility that Gas may act as an

indirect modulator of CB1R activation warrants further investigation, acknowledging the potential for non-linear signaling pathways.

The involvement of CB1R in the RhoA-related signaling pathway has been reported, with evidence suggesting both activation and inhibition of RhoA activity by CB1R in different cell types [33, 52, 66]. Additionally, RhoA has been implicated in mediating spinal cord regeneration in neurons and astrocytes, indicating cell-type-specific regulation of RhoA activity [67]. Previous studies reported that decreased RhoA expression alleviates both stroke injuries and depressive-like behaviors [31], and inhibition of the RhoA/ROCK pathway promotes adult hippocampal neurogenesis [68], suggesting a neuroprotective role of this pathway in the fascinating recovery of brain functions following brain injury, such as ischemia. The present study confirms CB1R's inhibitory effect on RhoA activity in the hippocampal CA1 area, consisting mainly of excitatory neurons. The inconsistency in CB1R's effect on RhoA activity across studies may stem from cell-specific regulation. Notably, our results show elevated RhoA activity and attenuated PKA activity upon decreased membrane CB1R expression in PSD mice, effectively reversed by Gas application. Local depletion of CB1R diminished the Gas-induced recovery, indicating the involvement of CB1R/PKA/RhoA signaling cascade in modulating stroke-induced depressive-like behaviors. Our findings suggest that targeting the PKA/RhoA signaling pathway may serve as a novel therapeutic strategy for PSD treatment.

Previous studies have underscored the critical role of spine morphogenesis and synaptogenesis in neurotransmission and synaptic plasticity [69]. The cytoskeleton, a crucial regulator of specialized neuronal structures, including dendritic spines, plays a fundamental role in neural communication [30, 70]. Studies have demonstrated that upregulation of RhoA activity leads to attenuation of dendritic spine morphogenesis and significant spine loss [71, 72]. The Rho family of small GTPases, acting as molecular switches, robustly controls cytoskeletal integrity, influencing synapse formation [73]. The RhoA/ROCK pathway, known for its involvement in cytoskeletal rearrangement, can induce neurogenesis changes and facilitate the survival of newborn neurons upon inhibition [28]. Combining the data, our findings suggest that membrane-bound CB1R inhibits RhoA activity via a pathway involving PKA. Reduced expression of CB1R results in the loss of this inhibitory effect on RhoA, leading to aberrant spine morphogenesis and synaptogenesis. We propose that impairment of the CB1R/PKA/RhoA signaling pathway could significantly contribute to the development of depression-like behaviors following stroke. It is plausible that Gas treatment recruits CB1R/PKA/RhoA signaling cascade to restore impaired spine morphogenesis and synaptogenesis in PSD. Thereby, it reconstitutes neurotransmission and synaptic plasticity, exerting its anti-PSD function.

Depression often coexists with conditions such as anxiety, diabetes, and pain, among other neuropsychiatric disorders. Various neurochemical systems, including dopaminergic, serotoninergic, opioidergic, and adrenergic systems, are well-recognized contributors to the pathogenesis of depression [74]. Given the diverse origins of depression, it is unlikely that CB1R/PKA/RhoA pathway impairment is the sole risk factor in the development of PSD. Indeed, robust evidence points to other risk factors playing a role in stroke-induced depression. CB1R forms heteromeric complexes with various receptors, including dopamine D2 receptors and serotonin receptors (5HT1A and 5HT2A), which have been implicated in the pathophysiology of depression [75–77]. The involvement of CB1R in diverse signaling pathways emphasizes its role in stress-related mental disorders and may contribute to the variations observed in the regulation of RhoA activity. Additionally, CB1R expression in astrocytes, forming tripartite synapses with neurons, highlights its modulation of pre- and post-synaptic elements during synaptic transmission [78, 79]. Animal studies have shown that the blockade of CB1R signaling leads to increased anxiety, stress maladaptation, and elevated hypothalamic-pituitary-adrenal axis activity [80]. These diverse findings underscore the complex activation patterns and molecular heterogeneity of CB1R in contributing to the progression or exacerbation of depression. Understanding the molecular and synaptic mechanisms underlying PSD is crucial for enhancing our comprehension of the intricate relationship between stroke and depression. This knowledge holds the potential to inspire tailored clinical treatments for these debilitating conditions.

There are limitations in this study. The administration of both 7-day and 14-day intravenous Gas treatments resulted in the alleviation of post-stroke depressive-like behaviors in stressed MCAO mice. However, due to the procedural challenges of intravenous injection, further experiments would be informative to explore whether an equivalent or extended application of Gas through intraperitoneal or oral administration produces comparable or distinct effects in mitigating depressive-like behaviors. Additionally, while studies have suggested that gender is a transient factor influencing the emergence of PSD in humans [81, 82], it has been observed that females are more prone to developing PSD in elderly stroke patients [83]. Conducting additional studies to explore the molecular mechanisms underlying age-dependent development of PSD will provide a detailed elucidation of the pathogenesis of stroke-related complications.

Conclusions

In conclusion, our findings collectively demonstrate the antidepressive effect of Gas in a rodent model of PSD. This effect is associated with a reduction in membrane CB1R expression and

the hyperactivation of RhoA, revealing interconnected signaling pathways that illuminate the crosstalk between ischemia and depression. The study underscores Gas's crucial roles in promoting an anti-depressive state, supporting synaptogenesis, and stabilizing the CB1R-RhoA pathway. Our research expands the potential clinical applications of Gas as a beneficial therapeutic target for PSD. We propose that Gas treatment could serve as a valuable alternative pharmacotherapy for adjunctive treatment in psychiatric diseases, including PSD. Further validation of the neuroprotective effects of Gas in future clinical trials is warranted.

Supplementary Information The online version contains supplementary material available at https://doi.org/10.1007/s12035-024-04267-5.

Acknowledgements We thank Xufei Chen for his help with molecular docking simulation.

Author Contributions Shiquan Wang, Minghui Wang, Wugang Hou and Xia Li contributed to the study conception and experimental design, Shiquan Wang, Liang Yu, Haiyun Guo, Yaru Guo, Huiqing Liu, Jiajia Wang and Wenqiang Zuo performed experiments, and Shiquan Wang, Jin Wang, and Wenqiang Zuo performed data collection and analysis. Minghui Wang and Shiquan Wang prepared figures. Minghui Wang, Shiquan Wang wrote the paper. All authors reviewed and approved the paper.

Funding This research was supported by the National Natural Science Foundation of China (no. 82271549 to MW; no. 81971226 to WH; no. 81901079 to HG), the Xi'an Innovative Project for Strengthening Basic Disciplines - Clinical Research Program (no. 22YXYJ0154 to MW); the Shaanxi Provincial Natural Science Foundation for Distinguished Young Scholars (no. 2021JC-33 to WH), and the Shaanxi Provincial Natural Science Foundation (no. 2023-JC-YB-652 to SW).

Data Availability No datasets were generated or analysed during the current study.

Declarations

Competing Interests The authors declare no competing interests.

References

1. Guo J, Wang J, Sun W, Liu X (2022) The advances of post-stroke depression: 2021 update. J Neurol 269:1236–1249
2. Robinson RG, Jorge RE (2016) Post-stroke Depression: a review. Am J Psychiatry 173:221–231
3. Villa RF, Ferrari F, Moretti A (2018) Post-stroke depression: mechanisms and pharmacological treatment. Pharmacol Ther 184:131–144
4. Choi-Kwon S, Han SW, Kwon SU, Kang D-W, Choi JM, Kim JS (2006) Fluoxetine Treatment in Poststroke Depression, emotional incontinence, and anger proneness: a Double-Blind, placebo-controlled study. Stroke 37:156–161
5. Fruehwald S, Gatterbauer E, Rehak P, Baumhackl U (2003) Early fluoxetine treatment of post-stroke depression. J Neurol 250:347–351
6. Ye T, Meng X, Wang R, Zhang C, He S, Sun G et al (2018) Gastrodin alleviates cognitive dysfunction and depressive-like behaviors by inhibiting ER stress and NLRP3 inflammasome activation in db/db mice. Int J Mol Sci 19:3977
7. Liu Y, Gao J, Peng M, Meng H, Ma H, Cai P et al (2018) A review on Central Nervous System effects of Gastrodin. Front Pharmacol 9:24
8. Chen W-C, Lai Y-S, Lin S-H, Lu K-H, Lin Y-E, Panyod S et al (2016) Anti-depressant effects of Gastrodia Elata Blume and its compounds gastrodin and 4-hydroxybenzyl alcohol, via the monoaminergic system and neuronal cytoskeletal remodeling. J Ethnopharmacol 182:190–199
9. Peng Z, Wang S, Chen G, cai M, Liu R, Deng J et al (2015) Gastrodin alleviates cerebral ischemic damage in mice by improving anti-oxidant and anti-inflammation activities and inhibiting apoptosis pathway. Neurochem Res 40:661–673
10. Ye T, Meng X, Zhai Y, Xie W, Wang R, Sun G et al (2018) Gastrodin ameliorates cognitive dysfunction in diabetes rat model via the suppression of endoplasmic reticulum stress and NLRP3 inflammasome activation. Front Pharmacol 9:1346
11. Li M, Qian S (2016) Gastrodin protects neural progenitor cells against amyloid β (1–42)-Induced neurotoxicity and improves hippocampal neurogenesis in amyloid β (1–42)-Injected mice. J Mol Neurosci 60:21–32
12. Wu F, Zuo H-J, Ren X-Q, Wang P-X, Li F, Li J-J (2023) Gastrodin regulates the Notch-1 Signal Pathway via renin–angiotensin system in activated Microglia. NeuroMolecular Med 25:40–52
13. Huang Q, Shi J, Gao B, Zhang H-Y, Fan J, Li X-J et al (2015) Gastrodin: an ancient Chinese herbal medicine as a source for anti-osteoporosis agents via reducing reactive oxygen species. Bone 73:132–144
14. Wang X, Zhang B, Li X, Liu X, Wang S, Xie Y et al (2021) Mechanisms underlying Gastrodin Alleviating Vincristine-Induced Peripheral Neuropathic Pain. Front Pharmacol 12:744663
15. Wang X, Li S, Ma J, Wang C, Chen A, Xin Z et al (2019) Effect of Gastrodin on Early Brain Injury and neurological outcome after subarachnoid hemorrhage in rats. Neurosci Bull 35:461–470
16. Li G, Ma Y, Ji J, Si X, Fan Q (2018) Effects of gastrodin on 5-HT and neurotrophic factor in the treatment of patients with post-stroke depression. Exp Ther Med 16:4493-4498
17. Xian-En Zhao, Yongrui He, Shuyun Zhu, Yanqiu Xu, Jinmao You, Yu Bai, Huwei Liu(2019) Stable isotope labeling derivatization and magnetic dispersive solid phase extraction coupled with UHPLC-MS/MS for the measurement of brain neurotransmitters in post-stroke depression rats administrated with gastrodin Analytica Chimica Acta,21:73-81
18. Medeiros GC, Roy D, Kontos N, Beach SR (2020) Post-stroke depression: a 2020 updated review. Gen Hosp Psychiatry 66:70–80
19. Pietri M, Djillani A, Mazella J, Borsotto M, Heurteaux C (2019) First evidence of protective effects on stroke recovery and post-stroke depression induced by sortilin-derived peptides. Neuropharmacology 158:107715
20. Bright U, Akirav I (2022) Modulation of Endocannabinoid System Components in Depression: pre-clinical and clinical evidence. Int J Mol Sci 23:5526
21. Chadwick VL, Rohleder C, Koethe D, Leweke FM (2020) Cannabinoids and the endocannabinoid system in anxiety, depression, and dysregulation of emotion in humans. Curr Opin Psychiatry 33:20–42
22. Duncan RS, Riordan SM, Gernon MC, Koulen P (2024) Cannabinoids and endocannabinoids as therapeutics for nervous system disorders: preclinical models and clinical studies. Neural Regen Res 19:788–799

23. Hasbi A, Madras BK, George SR (2023) Endocannabinoid System and Exogenous cannabinoids in Depression and anxiety: a review. Brain Sci 13:325
24. Hillard C, Liu Q (2014) Endocannabinoid Signaling in the etiology and treatment of major depressive illness. Curr Pharm Des 20:3795–3811
25. Shen C-J, Zheng D, Li K-X, Yang J-M, Pan H-Q, Yu X-D et al (2019) Cannabinoid CB1 receptors in the amygdalar cholecystokinin glutamatergic afferents to nucleus accumbens modulate depressive-like behavior. Nat Med 25:337–349
26. Soriano D, Brusco A, Caltana L (2021) Further evidence of anxiety- and depression-like behavior for total genetic ablation of cannabinoid receptor type 1. Behav Brain Res 400:113007
27. Wang S, Sun H, Liu S, Wang T, Guan J, Jia J (2016) Role of hypothalamic cannabinoid receptors in post-stroke depression in rats. Brain Res Bull 121:91–97
28. Briz V, Zhu G, Wang Y, Liu Y, Avetisyan M, Bi X et al (2015) Activity-dependent Rapid Local RhoA synthesis is required for hippocampal synaptic plasticity. J Neurosci 35:2269–2282
29. Amar M, Pramod AB, Yu N-K, Herrera VM, Qiu LR, Moran-Losada P et al (2021) Autism-linked Cullin3 germline haploinsufficiency impacts cytoskeletal dynamics and cortical neurogenesis through RhoA signaling. Mol Psychiatry 26:3586–3613
30. Van Aelst L, Cline HT (2004) Rho GTPases and activity-dependent dendrite development. Curr Opin Neurobiol 14:297–304
31. Zhou J, Ma Y, Chen J, Yao D, Feng C, Dong Y et al (2022) Effects of RhoA on depression-like behavior in prenatally stressed offspring rats. Behav Brain Res 432:113973
32. Lu W, Chen Z, Wen J (2021) RhoA/ROCK signaling pathway and astrocytes in ischemic stroke. Metab Brain Dis 36:1101–1108
33. Berghuis P, Rajnicek AM, Morozov YM, Ross RA, Mulder J, Urbán GM et al (2007) Hardwiring the brain: endocannabinoids shape neuronal connectivity. Science 316:1212–1216
34. Newell-Litwa KA, Horwitz AR (2011) Cell Migration: PKA and RhoA set the Pace. Curr Biol 21:R596–R598
35. Kim H-J, Choi H-S, Park J-H, Kim M-J, Lee H, Petersen RB et al (2017) Regulation of RhoA activity by the cellular prion protein. Cell Death Dis 8:e2668–e2668
36. Ma C-L, Li L, Yang G-M, Zhang Z-B, Zhao Y-N, Zeng X-F et al (2020) Neuroprotective effect of gastrodin in methamphetamine-induced apoptosis through regulating cAMP/PKA/CREB pathway in cortical neuron. Hum Exp Toxicol 39:1118–1129
37. Gao F, Yang S, Wang J, Zhu G (2022) cAMP-PKA cascade: an outdated topic for depression? Biomed Pharmacother Biomedecine Pharmacother 150:113030
38. Kim MH, Leem YH (2014) Chronic exercise improves repeated restraint stress-induced anxiety and depression through 5HT1A receptor and cAMP signaling in hippocampus. J Exerc Nutr Biochem 18:97–104
39. Zhang G, Chen L, Yang L, Hua X, Zhou B, Miao Z et al (2015) Combined use of spatial restraint stress and middle cerebral artery occlusion is a novel model of post-stroke depression in mice. Sci Rep 5:16751
40. Wang S, Zhang Z, Wang J, Ma L, Zhao J, Wang J et al (2022) Neuronal GPER participates in genistein-mediated neuroprotection in ischemic stroke by inhibiting NLRP3 inflammasome activation in Ovariectomized Female Mice. Mol Neurobiol 59:5024–5040
41. Vahid-Ansari F, Lagace DC, Albert PR (2016) Persistent post-stroke depression in mice following unilateral medial prefrontal cortical stroke. Transl Psychiatry 6:e863
42. Verma R, Friedler BD, Harris NM, McCullough LD (2014) Pair housing reverses post-stroke depressive behavior in mice. Behav Brain Res 269:155–163
43. Zhao Y, Martins-Oliveira M, Akerman S, Goadsby PJ (2018) Comparative effects of traditional Chinese and western migraine medicines in an animal model of nociceptive trigeminovascular activation. Cephalalgia Int J Headache 38:1215–1224
44. Wen J-Y, Gao S-S, Chen F-L, Chen S, Wang M, Chen Z-W (2019) Role of CSE-Produced H2S on cerebrovascular relaxation via RhoA-ROCK inhibition and cerebral ischemia-reperfusion Injury in mice. ACS Chem Neurosci 10:1565–1574
45. Zhang Y, Yan J, Xu H, Yang Y, Li W, Wu H et al (2018) Extremely low frequency electromagnetic fields promote mesenchymal stem cell migration by increasing intracellular Ca2 + and activating the FAK/Rho GTPases signaling pathways in vitro. Stem Cell Res Ther 9:143
46. Başaran N, Paslı D, Başaran AA (2022) Unpredictable adverse effects of herbal products. Food Chem Toxicol 159:112762
47. Haj-Mirzaian A, Amini-Khoei H, Haj-Mirzaian A, Amiri S, Ghesmati M, Zahir M et al (2017) Activation of cannabinoid receptors elicits antidepressant-like effects in a mouse model of social isolation stress. Brain Res Bull 130:200–210
48. Kolb B, Saber H, Fadel H, Rajah G (2019) The endocannabinoid system and stroke: a focused review. Brain Circ 5:1
49. Zou S, Kumar U (2018) Cannabinoid receptors and the Endocannabinoid System: signaling and function in the Central Nervous System. Int J Mol Sci 19:833
50. Wilson RI, Nicoll RA (2001) Endogenous cannabinoids mediate retrograde signalling at hippocampal synapses. Nature 410:588–592
51. Puighermanal E, Marsicano G, Busquets-Garcia A, Lutz B, Maldonado R, Ozaita A (2009) Cannabinoid modulation of hippocampal long-term memory is mediated by mTOR signaling. Nat Neurosci 12:1152–1158
52. Mai P, Tian L, Yang L, Wang L, Yang L, Li L (2015) Cannabinoid receptor 1 but not 2 mediates macrophage phagocytosis by $G_{(\alpha)i/o}$/RhoA/ROCK signaling pathway: CANNABINOID RECEPTORS/MACROPHAGE PHAGOCYTOSIS. J Cell Physiol 230:1640–1650
53. Tkachenko E, Sabouri-Ghomi M, Pertz O, Kim C, Gutierrez E, Machacek M et al (2011) Protein kinase a governs a RhoA–RhoGDI protrusion–retraction pacemaker in migrating cells. Nat Cell Biol 13:660–667
54. Kronenberg G, Balkaya M, Prinz V, Gertz K, Ji S, Kirste I et al (2012) Exofocal Dopaminergic Degeneration as Antidepressant Target in Mouse Model of Poststroke Depression. Biol Psychiatry 72:273–281
55. Zahrai A, Vahid-Ansari F, Daigle M, Albert PR (2020) Fluoxetine-induced recovery of serotonin and norepinephrine projections in a mouse model of post-stroke depression. Transl Psychiatry 10:334
56. Gallego-Landin I, García-Baos A, Castro-Zavala A, Valverde O (2021) Reviewing the role of the Endocannabinoid System in the pathophysiology of Depression. Front Pharmacol 12:762738
57. Marwaha S, Palmer E, Suppes T, Cons E, Young AH, Upthegrove R (2023) Novel and emerging treatments for major depression. Lancet 401:141–153
58. Malhi GS, Mann JJ, Depression (2018) Lancet 392:2299–2312
59. Richter D, Charles James J, Ebert A, Katsanos AH, Mazul-Wach L, Ruland Q et al (2021) Selective serotonin reuptake inhibitors for the Prevention of Post-stroke Depression: a systematic review and Meta-analysis. J Clin Med 10:5912
60. Lee B, Sur B, Yeom M, Shim I, Lee H, Hahm D-H (2016) Gastrodin reversed the traumatic stress-induced depressed-like symptoms in rats. J Nat Med 70:749–759
61. Murillo-Rodriguez E, Pandi-Perumal SR, Monti JM (eds) (2021) Cannabinoids and Neuropsychiatric disorders. Springer International Publishing, Cham
62. Cai M, Yang Q, Li G, Sun S, Chen Y, Tian L et al (2017) Activation of cannabinoid receptor 1 is involved in protection against mitochondrial dysfunction and cerebral ischaemic tolerance induced by isoflurane preconditioning. Br J Anaesth 119:1213–1223

63. Takahashi KA, Castillo PE (2006) The CB1 cannabinoid receptor mediates glutamatergic synaptic suppression in the hippocampus. Neuroscience 139:795–802
64. Siraj MA, Rahman Md, Tan G, Seidel V (2021) Molecular Docking and Molecular Dynamics Simulation Studies of Triterpenes from Vernonia patula with the cannabinoid type 1 receptor. Int J Mol Sci 22:3595
65. Haspula D, Clark MA (2020) Cannabinoid receptors: an update on Cell Signaling, Pathophysiological roles and Therapeutic opportunities in Neurological, Cardiovascular, and Inflammatory diseases. Int J Mol Sci 21:7693
66. Sánchez-de la Torre A, Aguado T, Huerga-Gómez A, Santamaría S, Gentile A, Chara JC et al (2022) Cannabinoid CB1 receptor gene inactivation in oligodendrocyte precursors disrupts oligodendrogenesis and myelination in mice. Cell Death Dis 13:585
67. Stern S, Hilton BJ, Burnside ER, Dupraz S, Handley EE, Gonyer JM et al (2021) RhoA drives actin compaction to restrict axon regeneration and astrocyte reactivity after CNS injury. Neuron 109:3436–3455e9
68. Christie KJ, Turbic A, Turnley AM (2013) Adult hippocampal neurogenesis, rho kinase inhibition and enhancement of neuronal survival. Neuroscience 247:75–83
69. Li Z, Okamoto K-I, Hayashi Y, Sheng M (2004) The importance of dendritic mitochondria in the Morphogenesis and plasticity of spines and synapses. Cell 119:873–887
70. Govek E-E, Newey SE, Van Aelst L (2005) The role of the rho GTPases in neuronal development. Genes Dev 19:1–49
71. Luo L, Hensch TK, Ackerman L, Barbel S, Jan LY, Nung Jan Y (1996) Differential effects of the rac GTPase on Purkinje cell axons and dendritic trunks and spines. Nature 379:837–840
72. Tashiro A (2000) Regulation of dendritic spine morphology by the rho family of small GTPases: antagonistic roles of Rac and Rho. Cereb Cortex 10:927–938
73. Maletic-Savatic M, Malinow R, Svoboda K (1999) Rapid dendritic morphogenesis in CA1 hippocampal dendrites Induced by synaptic activity. Science 283:1923–1927
74. Herrman H, Patel V, Kieling C, Berk M, Buchweitz C, Cuijpers P et al (2022) Time for united action on depression: a Lancet–World Psychiatric Association Commission. Lancet 399:957–1022
75. Kearn CS, Blake-Palmer K, Daniel E, Mackie K, Glass M (2005) Concurrent stimulation of cannabinoid CB1 and dopamine D2 receptors enhances heterodimer formation: a mechanism for receptor cross-talk? Mol Pharmacol 67:1697–1704
76. Marcellino D, Carriba P, Filip M, Borgkvist A, Frankowska M, Bellido I et al (2008) Antagonistic cannabinoid CB1/dopamine D2 receptor interactions in striatal CB1/D2 heteromers. A combined neurochemical and behavioral analysis. Neuropharmacology 54:815–823
77. Zhang M, Mahadevan A, Amere M, Li H, Ganea D, Tuma RF (2012) Unique effects of compounds active at both cannabinoid and serotonin receptors during stroke. Transl Stroke Res 3:348–356
78. Castillo PE, Younts TJ, Chávez AE, Hashimotodani Y (2012) Endocannabinoid signaling and synaptic function. Neuron 76:70–81
79. Navarrete M, Araque A (2010) Endocannabinoids potentiate synaptic transmission through stimulation of astrocytes. Neuron 68:113–126
80. Zhou L, Wang T, Yu Y, Li M, Sun X, Song W et al (2022) The etiology of poststroke-depression: a hypothesis involving HPA axis. Biomed Pharmacother 151:113146
81. Poynter B, Shuman Hon M, Diaz-Granados N, Kapral M, Grace SL, Stewart DE (2009) Sex differences in the prevalence of Post-stroke Depression: a systematic review. Psychosomatics 50:563–569
82. Volz M, Ladwig S, Werheid K (2021) Gender differences in post-stroke depression: a longitudinal analysis of prevalence, persistence and predictive value of known risk factors. Neuropsychol Rehabil 31:1–17
83. Mayman NA, Tuhrim S, Jette N, Dhamoon MS, Stein LK (2021) Sex differences in Post-stroke Depression in the Elderly. J Stroke Cerebrovasc Dis 30:105948